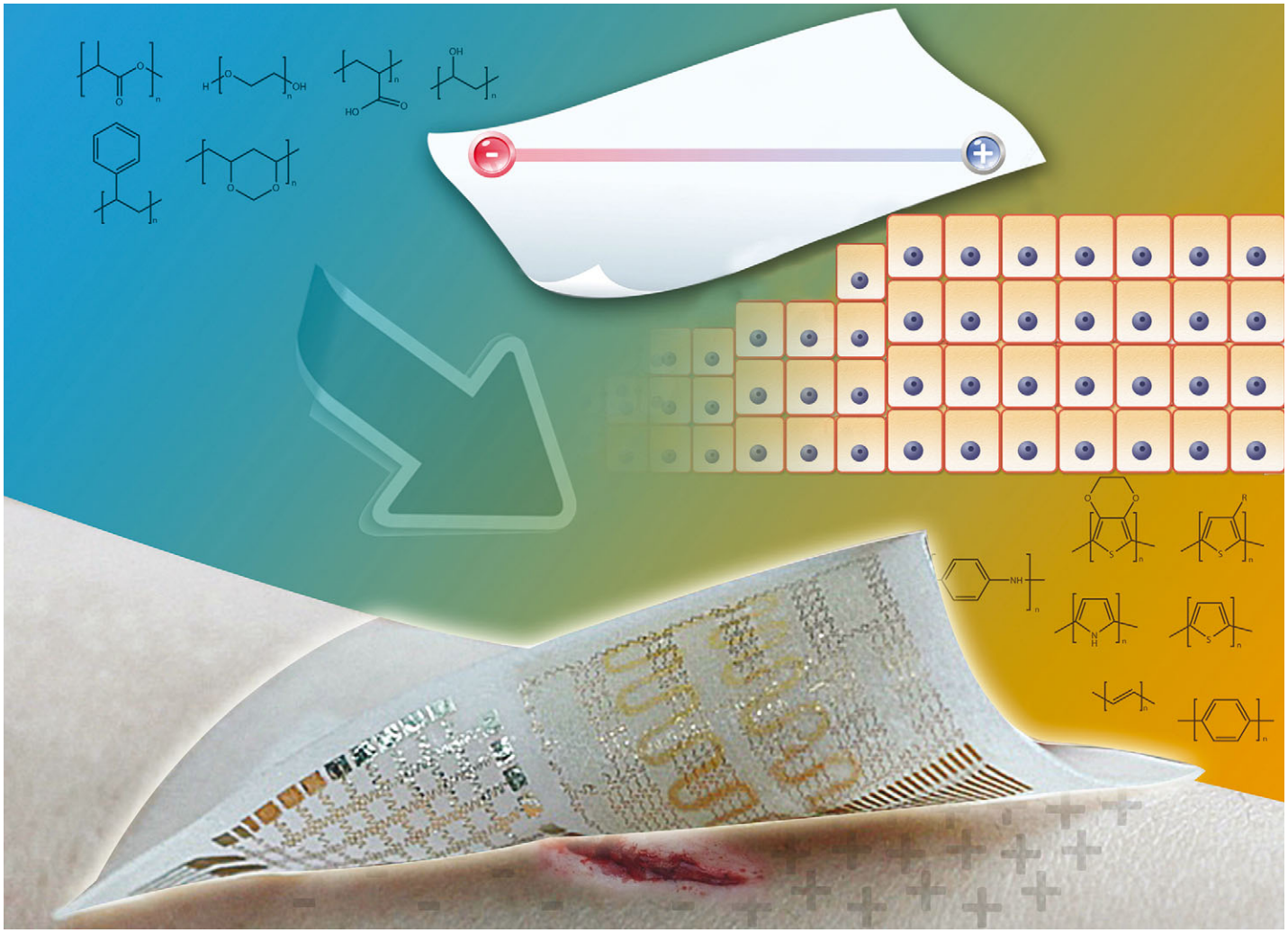

Showcasing research on free-standing nanomembranes for advanced biomedical applications reviewed by Prof. Jordi Puiggalí and Prof. Carlos Alemán from the Chemical Engineering Department of Universitat Politècnica de Catalunya, Spain.

Insulating and semiconducting polymeric free-standing nanomembranes with biomedical applications

This work reviews the most recent examples on free-standing nanomembranes as versatile elements in biotechnological applications. Their design is evolving from being composed of insulating (bio)polymers to also incorporating electroactive conducting polymers that add electrochemical and electrical functionalities to the system.

Image adapted by permission from Macmillan Publishers Ltd: *Nat. Nanotechnol.*, 2014, **9**, 397–404.

As featured in:

See Maria M. Pérez-Madrigal, Carlos Alemán *et al.*, *J. Mater. Chem. B*, 2015, **3**, 5904.

ROYAL SOCIETY OF CHEMISTRY

www.rsc.org/MaterialsB

Registered charity number: 207890

Journal of
Materials Chemistry B

REVIEW

View Article Online
View Journal | View Issue

CrossMark
click for updates

Cite this: J. Mater. Chem. B, 2015, 3, 5904

Insulating and semiconducting polymeric free-standing nanomembranes with biomedical applications

Maria M. Pérez-Madrigal,*[ab] Elaine Armelin,[ab] Jordi Puiggalí[ab] and Carlos Alemán*[ab]

Received 6th April 2015,
Accepted 28th May 2015

DOI: 10.1039/c5tb00624d

www.rsc.org/MaterialsB

In recent decades, polymers have experienced a radical evolution: from being used as inexpensive materials in the manufacturing of simple appliances to be designed as nanostructured devices with important applications in many leading fields, such as biomedicine at the nanoscale. Within this context, polymeric free-standing nanomembranes – self-supported quasi-2D structures with a thickness ranging from ~10 to a few hundreds of nanometers and an aspect ratio of size and thickness greater than 10^6 – are emerging as versatile elements for applications as varied as overlapping therapy, burn wound infection treatment, antimicrobial platforms, scaffolds for tissue engineering, drug-loading and delivery systems, biosensors, *etc.* Although at first, a little over a decade ago, materials for the fabrication of free-standing nanosheets were limited to biopolymers and insulating polymers that were biodegradable, during the last five years the use of electroactive conducting polymers has been attracting much attention because of their extraordinary advantages in the biomedical field. In this context, a systematic review of current research on polymeric free-standing nanomembranes for biomedical applications is presented. Moreover, further discussion on the future developments of some of these exciting areas of study and their principal challenges is presented in the conclusion section.

Open Access Article. Published on 28 May 2015. Downloaded on 4/2/2026 11:03:23 AM.
This article is licensed under a Creative Commons Attribution 3.0 Unported Licence.

1. Introduction

Over the past few decades, biomaterials science has been increasingly evolving into a more interdisciplinary field combining elements of medicine, chemistry, biology, engineering and materials science. Recently, nanotechnological concepts

[a] *Departament d'Enginyeria Química, ETSEIB, Universitat Politècnica de Catalunya, Avda. Diagonal 647, Barcelona E-08028, Spain. E-mail: m.mar.perez@upc.edu, carlos.aleman@upc.edu*
[b] *Center for Research in Nano-Engineering, Universitat Politècnica de Catalunya, Campus Sud, Edifici C', C/Pasqual i Vila s/n, Barcelona E-08028, Spain*

Maria M. Pérez-Madrigal

Maria M. Pérez-Madrigal received her BSc degree in Chemical Engineering (2010) and her MSc degree in Polymers and Biopolymers (2011) at the Universitat Politècnica de Catalunya (UPC), Barcelona, Spain. She is currently a PhD student under the supervision of Prof. Carlos Alemán and Dr Elaine Armelin. Her research focuses on combining conducting polymers with conventional polymers to obtain biointerfaces at the nanoscale (nanomembranes and nanofibers) for applications such as tissue engineering scaffolds or drug-delivery systems.

Elaine Armelin

Elaine Armelin is Associate Professor in the Chemical Engineering Department and the Center for Research in NanoEngineering (CRnE), Universitat Politècnica de Catalunya (UPC, Spain). She received her Bachelor's degree in Chemistry in 1995 and Master Degree in Organic Chemistry in 1997 at the Universidade de São Paulo (USP-Brazil). In 1997 she moved to Barcelona to perform her PhD studies in Polymer Science, under the supervision of Prof. Puiggalí, at the UPC. She is a co-author of more than 80 peer reviewed publications and patents. Her main interests are characterization of polymeric materials and corrosion protection by using organic–inorganic coatings.

This journal is © The Royal Society of Chemistry 2015

Open Access Article. Published on 28 May 2015. Downloaded on 4/2/2026 11:03:23 AM.
This article is licensed under a Creative Commons Attribution 3.0 Unported Licence.

and procedures have also been applied to obtain and improve devices with very different applications in biomedicine and biotechnology.[1–3] Specifically, there is growing interest in the fabrication of nanomembranes (also known as ultra-thin films or nanosheets) since their distinctive features make them suitable for designing sensors,[4,5] nanobiological reactors,[6] biomotors,[7] biointerfaces for cellular matrices,[8] antimicrobial surfaces,[9,10] or drug release devices.[11,12] In practice, the term *nanomembrane* refers to quasi-2D structures with macroscopic surface area and thickness values ranging from 10 to a few hundreds of nm. A few years ago, Kunitake *et al.*,[13] pioneers in this field, coined the term "*giant nanomembrane*" to denote self-supporting (namely, free-standing) membranes with thickness from 1 to 100 nm and an aspect ratio of size and thickness greater than 10^6. Such a high aspect ratio facilitates the handling of these nanomembranes, while the self-supporting properties, which enable the nanosheet to be removed from its supporting substrate retaining the mechanical integrity, are required to physically separate two spaces. Besides, free-standing nanomembranes (hereafter denoted as FsNMs) are characterized by other special properties, such as low weight, high flexibility, robustness, and, in some cases, transparency.[14]

Research on FsNMs for biomedical applications started less than a decade ago when it was proved that ultra-thin sheets prepared using biodegradable and biocompatible polyesters and polysaccharides exhibited excellent mechanical properties and adhesion strength. Rapidly, this led to considerable interest in these nanosheets as novel substrate/biointerfaces to promote cell adhesion, migration, proliferation and differentiation. More recently, FsNMs have been used for different therapeutic uses, for example treatment of microbial infections, control of cell adhesion and repair of tissue defects. In this review, we discuss the most representative examples of FsNMs made of insulating and electrochemically inactive polymers for advanced biomedical applications. After this, we present the very recent achievements in the application of electroactive conducting polymers (ECPs) what we call the "*second generation of FsNMs*", which incorporate electrochemical and electrical functionalities for biomedical applications. Before such a discussion, brief explanations about the different strategies that can be used to fabricate FsNMs and the main concepts of ECPs are provided.

2. Preparation of free-standing nanomembranes

Typically, FsNMs are produced by depositing nanofilms on solid substrates, or *via* fluid–fluid or liquid–air interfaces. In addition, some other approaches, including layer-by-layer (LbL) assembly,[15–17] Langmuir–Blodgett transfer (LB),[18] spin-coating,[19] electrophoretic deposition[20] and cross-linking of self-assembled monolayer (SAM) techniques,[21] are also often employed. These methods differ in two general aspects: (1) the degree of control over the final FsNM thickness, composition and stability; and (2) the step in which the nanomembrane is removed, transferred or extracted from the solid surface or the fluid–fluid interface.[22]

In the LbL technique, which was developed by Decher *et al.*[15–17] in the early 1990s, the formation of the FsNM is achieved by depositing on a solid surface alternating layers of oppositely charged materials (Fig. 1a), such as polyions, metals, nanoparticles, ceramics or biological molecules. Accordingly, FsNM stability arises from primary or secondary interactions between those layers. This approach stands out because of its simplicity and the high degree of control over the FsNM thickness. Furthermore, the precise guidance exerted over the chemical composition of the layers results in a tremendous versatility when designing FsNMs.[23] Regarding the SAM technique, Stroock *et al.*[21] extensively described the synthesis of

Jordi Puiggalí

Jordi Puiggalí is a Full Professor at the Chemical Engineering Department of the Universitat Politècnica de Catalunya. He is the head of the "Macromolecular Chemistry" and "Synthetic Polymers, Structure and Properties" research groups. He also belongs to the Centre of Research on NanoEngineering, being the co-director of the laboratory of Nanochemistry. The main objectives of his research concern the development of new polymers and nanocomposites for biomedical applications, the structural studies of semicrystalline polymers and finally the study of crystallization processes and their influence on materials properties. His work has resulted in more than 200 articles and book chapters.

Carlos Alemán

Carlos Alemán earned his PhD in Chemistry at the Universitat Politècnica de Catalunya in 1994. He is currently Full Professor of Physical Chemistry in the same University, leading the "Innovation in Materials and Molecular Engineering" (IMEM) group in Chemical Engineering Department, and co-leading with Prof. J. Puiggalí the "Nanochemistry" group in the Centre of Research on Nano-Engineering. His main research interests focus on conducting polymers for biomedical applications, peptides as materials and development of peptide–polymer conjugates and composites. He is the author or co-author of over 450 review articles, research papers and book chapters.

Open Access Article. Published on 28 May 2015. Downloaded on 4/2/2026 11:03:23 AM.
This article is licensed under a Creative Commons Attribution 3.0 Unported Licence.

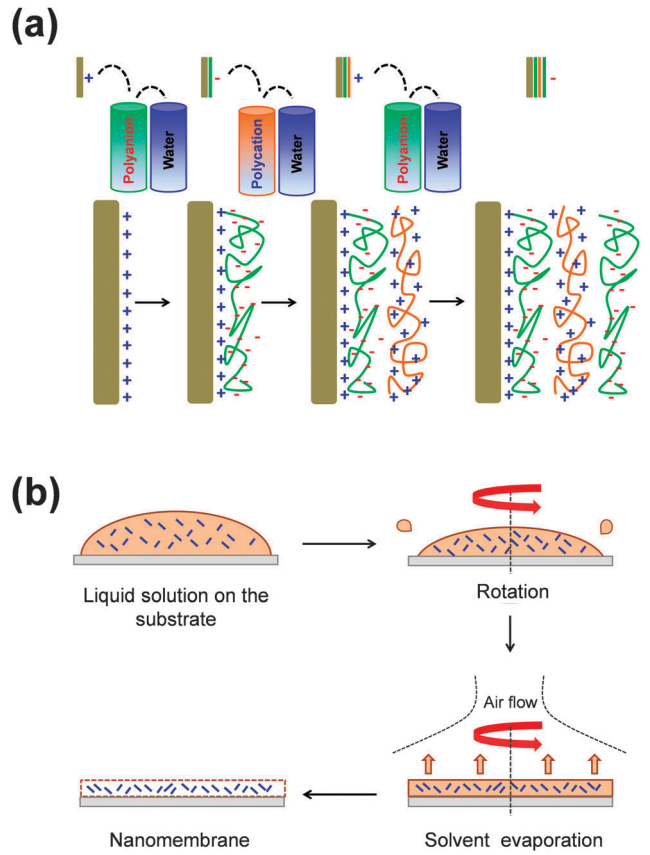

Fig. 1 Schematic illustration of the (a) LbL and (b) spin-coating processes.

polymeric FsNMs with 10–15 nm in thickness and well-defined lateral size and shape.

On the other hand, spin-coating (Fig. 1b) is another interesting approach that allows the preparation of single- or multi-layered FsNMs in a few steps. In this case, the optimization of the spin-coating parameters (*e.g.* spinning speed and time, and the solution concentration) leads to ultra-thin films with controlled features, thickness and homogeneity. In this procedure, which seems to be the most versatile and easy-going, the liquid polymeric solution is spin-coated onto a solid substrate previously coated with a sacrificial layer. Hence, by dissolving the sacrificial layer in an appropriate solvent, the FsNM is detached from the substrate and released into a liquid environment where it can be then easily handled using syringes or pipettes. Most of the FsNMs described in this review were fabricated using a combination of both the LbL assembly and spin-coating procedures.

3. Electroactive conducting polymers

Electroactive conducting polymers (ECPs) are widely known to be electrochemically active organic semiconducting materials. These polymers are special in that they consist of long conjugated polymeric chains that present alternation of double and single-bonded sp^2 hybridized atoms. This conjugation, which is described in terms of electronic wave functions that are delocalized over the entire chain, allows charge mobility along the polymer backbone and between adjacent chains, thus endowing the polymer with semiconductive and electrochemical properties.[24–26] Although the band structure of ECPs is similar to that of inorganic semiconductors, they also exhibit some of the attractive properties associated with conventional polymers (*i.e.* electrically insulating polymers), such as ease of synthesis and flexibility in processing. However, the mechanical stability of ECPs is typically lower than that of both inorganic semiconductors and conventional polymers.

The doping process converts neutral ECPs into semiconductive. In this process, the ECP is oxidized (p-doping) or reduced (n-doping) and, as a result, positive or negative charge carriers, respectively, are introduced into the backbone. Backbone charge carriers, which typically consist of charged polarons (*i.e.* radical cations or anions) or bipolarons (*i.e.* dications or dianions),[27] are accompanied by counter ions with opposite charges that are entrapped into the polymer matrix to maintain electrical neutrality. Simultaneously, the band structure of the ECP is modified to accommodate the formation of polaronic and bipolaronic bands, which facilitate the electrical conduction.

Although Bolto *et al.*[28] reported in 1963 polypyrrole derivatives with a resistivity as low as 1 Ohm cm, the discovery and development of conducting polymers were attributed to Shirakawa, MacDiarmid, and Heeger, who reported the conductivity of polyacetylene doped with iodine,[29] when they awarded with the Novel Prize in Chemistry 2000. Generally, ECPs are categorized into three groups: non-cyclic polyenes (*e.g.* polyacetylene), cyclic polyenes (*e.g.* poly(*p*-phenylene) and its derivatives), and polyheterocyclic ECPs (*e.g.* polypyrrole (PPy), polythiophene (PTh), and polyaniline (PAni)). The last group is actually considered the most versatile due to the excellent properties exhibited by such ECPs, especially in terms of electrochemical and environmental stabilities. Fig. 2 displays the chemical structure of the most representative ECP of each group.

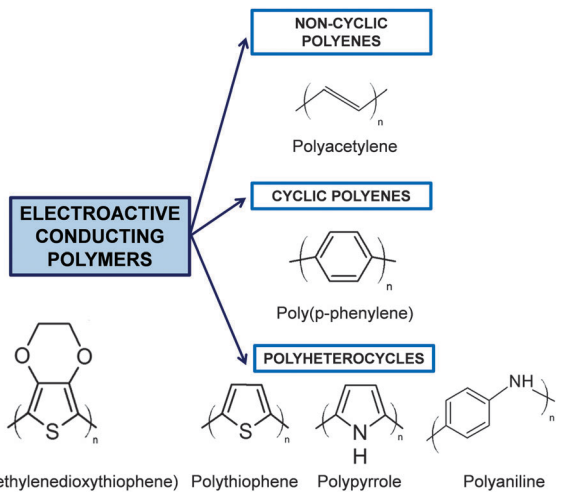

Fig. 2 General classification of ECPs and chemical structure of the most representative compounds of each group.

This journal is © The Royal Society of Chemistry 2015

Open Access Article. Published on 28 May 2015. Downloaded on 4/2/2026 11:03:23 AM.
This article is licensed under a Creative Commons Attribution 3.0 Unported Licence.

Table 1 Comparison of the chemical and electrochemical polymerization processes for the preparation of ECPs

Polymerization method	Advantages	Disadvantages
Chemical	– Large-scale production – Easy post-incorporation of other molecules to modify the ECP covalently – Many options to modify the chemical structure	– The synthetic process is more complicated than the electrochemical one – Preparation of ultra-thin films becomes a difficult task
Electrochemical	– Ease of synthesis – Entrapment of molecules in the polymer network becomes an easy process – The synthetic and doping processes occur simultaneously – Very useful to prepare ultra-thin films of controlled thickness	– Removal of the films from the electrode surface is frequently a very difficult task. – Post-covalent modification of ECPs is quite complex or, even, impossible

Although chemical synthesis provides many different possible routes to obtain a variety of ECPs, electrochemical synthesis is frequently the preferred alternative since this procedure is relatively straightforward and enables the control over the yield, morphology and electrochemical properties of the resulting material. Some ECPs, such as PPy and poly(3,4-ethylenedioxythiophene) (PEDOT), have been polymerized by both chemical and electrochemical processes, the advantages and disadvantages of both strategies are summarized in Table 1. Both procedures involve the oxidative polymerization of monomers dissolved in the medium by the action of a chemical oxidant or by applying an anodic potential at the electrode, respectively. The oxidative mechanism for polyheterocyclic ECPs, occurring in chemical and electrochemical polymerization processes, is summarized in Fig. 3.

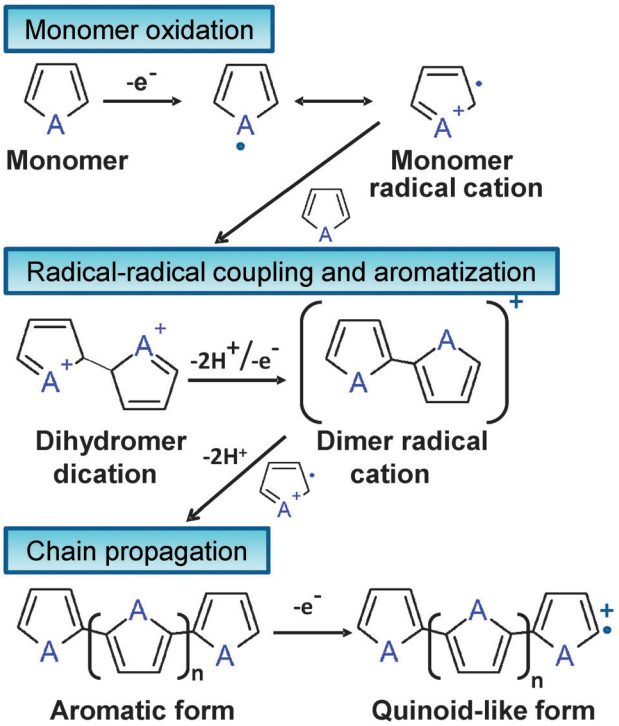

Fig. 3 Mechanism for heterocyclic ECPs polymerization, A = N–H and S for PPy and PTh, respectively.

Because of the outstanding electrical, electrochemical, optical and magnetic properties shown by ECPs,[24–26] these materials have been applied in a great number of technological fields that include organic optoelectronics,[30] organic photovoltaics,[31] energy storage technology,[32,33] and the fabrication of electrochromic[34] and electroluminescent[35] devices. Recently, as ECPs have also extended to biotechnological, bioengineering and biomedical fields,[36–39] special attention has been paid to tailor desirable properties (*i.e.* electrical, chemical and physical properties) to better suit the nature of the specific bioapplication. For example, the ability to entrap and controllably release biological molecules through reversible doping, and the ability to transfer charges from a biochemical reaction are two of the promising inherent functions of ECPs.

Currently, ECPs are frequently used as biosensors, tissue-engineering scaffolds, neural probes, drug-delivery devices and bio-actuators, as has been recently reviewed.[36–40] In particular, for tissue engineering applications, ECPs show interesting advantages but also some limitations (*i.e.* hydrophobicity, the lack of mechanical integrity and the absence of biodegradability).[37,40–42] ECP blending with conventional insulating polymers or biopolymers is the most popular approach followed to solve these drawbacks.[43–48] An alternative and also effective strategy, which was recently reviewed by Albertsson and co-workers,[43] is the synthesis of new biodegradable polymers containing conducting oligomers. Due to the growing interest in this class of new biomaterials, the palette of degradable and electrically conductive polymers is progressively expanding to meet the demands of specific applications within the biomedical field. For example, in the last year Schmidt and co-workers reported biodegradable electroactive copolymers composed of oligoaniline-based blocks linked to polyethylene glycol or polycaprolactone blocks, which deliver anti-inflammatory drugs upon application of electrochemical stimuli.[49]

In this work we use the concepts discussed in the two previous sections to review the fabrication of FsNMs for biomedical applications. Firstly, we will discuss the design and development of FsNMs made of biopolymers and insulating polymers. After this, we will focus on FsNMs fabricated by blending conventional polymers with ECPs. Finally, several concluding remarks on the achievements and future perspectives of this outstanding research field will be exposed.

Open Access Article. Published on 28 May 2015. Downloaded on 4/2/2026 11:03:23 AM.
This article is licensed under a Creative Commons Attribution 3.0 Unported Licence.

Table 2 Summary of the most important characteristics (*i.e.* preparation method, thickness, properties and potential biomedical applications) of FsNMs made of insulating and electrochemically inactive polymers

Material	Preparation	Thickness (nm)	Properties[a]	Biomedical applications	Ref.
PLA	Spin-coating	23 ± 5	E: 1.7 ± 0.1 GPa, L_c = (1.7 ± 0.3–1.8 ± 0.2) × 10^{-5} N m^{-1}. Transparency	Wound dressing, and atraumatic fixation tools	56–58
PLA	Spin-coating assisted multilayering	60 ± 6	Transparency	Barrier against burn wound infection	59
PLA	Spin-coating	320 ± 27	E: 136 ± 44 MPa. Transparency	Patch for bone or tendon repair and healing, and adhesive bioactive matrices for cell anchoring, spreading and proliferation	60 and 61
PLA-meshes	Spin-coating with the nanosheet collected on a stainless steel mesh	From 29 ± 1 to 703 ± 4.4	E: from 3.5 ± 1.3 to 7–10 GPa. Transparency. Weak adhesiveness for higher thickness nanosheets	Tailorable environment for anisotropic cell proliferation and differentiation without using conventional photolithographic approaches	62
PLA coated with collagen at one side	Spin-coating	59.5 ± 9.5 (PLA) and 5–10 (collagen)	Weak adhesiveness	Scaffolds that endow each side of the nanosheet with different discrete functions: anti-adhesive and pro-healing	63
PLA + SPION	Spin-coating	From 33 ± 3 to 245 ± 9	E similar to PLA. Magnetically responsive and colored	Magnetically controllable support	64
PLA–PAH–D–HA	Spin-coating + LbL	∼500 nm	Robust and flexible	Drug delivery	65
PLGA	Thermal fusion of adsorbed nanoparticles	—	—	Platelet substitutes and carriers	66
Chitosan–Na-alginate	Spin-coating assisted LbL	From 30.2 ± 4.3 to ∼75	E = 1.3/9.6 GPa. Pressure resistance, high flexibility and adhesiveness, transparency, biodegradability and semi-absorbent ability	Nano-adhesive plasters for tissue surfaces. Tissue defect repair without chemical bonding agents. Multi-overlapping therapy for venous hemorrhage. Arachnoid plasters in microsurgery without using chemical bonding agents.	68–71, 74 and 75
PVA–TC–(chitosan–Na-alginate)	Spin-coating assisted LbL	177	High flexibility, adhesive strength and transparency	Overlapping therapy, treatment of burn wound infections, antimicrobial platforms and drug-loading	72 and 73
HA–collagen	LbL	42 ± 4 (fibrous collagen) and 62 ± 7 (non-fibrous collagen)	For fibrous collagen: E = 12.5 ± 1.5 GPa, σ_{max} = 289 ± 9 MPa and ε_{max} = 1.0 ± 0.1%. For non-fibrous collagen: E = 4.3 ± 0.6 GPa, σ_{max} = 227 ± 10 MPa and ε_{max} = 1.7 ± 0.3%	Scaffolds for regenerative medicine	76
Cell–gelatin–$(chitosan–Na-alginate)_3$	LbL onto cultured cells on PNIPAM-grafted surfaces	—	—	Fabrication of complex artificial soft tissues to substitute some elements of native tissues	78
PEO–PAA	LbL	80 nm per bilayer	Elastomeric properties, smooth to touch and transparent	Biosubstrates, drug delivery devices and pH-sensitive sensors	85

This journal is © The Royal Society of Chemistry 2015

Open Access Article. Published on 28 May 2015. Downloaded on 4/2/2026 11:03:23 AM.
This article is licensed under a Creative Commons Attribution 3.0 Unported Licence.

Table 2 (*continued*)

Material	Preparation	Thickness (nm)	Properties[a]	Biomedical applications	Ref.
PAA–PEG–PAH–PSS	Spraying polymer solutions	55 to several hundreds	Components biocompatible, biotolerant or bioinert. Transparent and pH responsive	Therapeutic devices and aids	86
NBPT–PEG	Spin-coating	~5	Mechanical stability, biocompatibility and high transparency. Protein-repelling behavior	Support in transmission electron microscopy studies in their specific application to sensitive biological targets	87
PEG	Chemical cross-linking of a hydrogel precursor	10–350	Mechanical stability, high flexibility (E = ~2 MPa), hydrophilicity, and biorepulsion	Highly sensitive support and sensor elements for biological samples	88
PAH–PAA	LbL dipping + pH treatment for the creation of pores	253–688	Pores with diameters ranging from 300 nm to 2 μm (average: 1 μm)	Drug-delivery systems tuned by varying the number of layers and the pore size.	11
PDDA–P4VPPS	LbL	~29 per bilayer	pH-dependence, disintegration in alkali environments	Support (sacrificial layers) for biological templates	92
PHEMA	Surface-initiated ATRP on a PDA layer	16–75	Good chemical stability, low mechanical strength, transparency and colorless	Multi-stimuli responsive sensors after functionalizing the surface of the films	94
PMPC–(PS, PAH, PAA)	ATRP of MPC and spin-coating assisted LbL	11 (PMPC) + 85 ± 2 (PS, PAH, PAA)	Physiological stability, surface wettability and anti-biofouling	Biointerface for tissue-engineering scaffolds	95
PMMA	Spin-coating	199 ± 20	High flexibility, physiological stability and expected mechanical behavior similar to those of PLA FsNMs	Fabrication of platforms with space-selective cell culture environments by inject printing protein microarrays at the surface. Cell-directed culture in muscular tissue engineering	96
PMMA	Spin-coating PMMA : PS mixtures	From 38.8 ± 1.1 to 110.2 ± 2.0 nm	Porous and perforated structures	Potential applications in cell culture devices, high flux biosensors and drug delivery systems	97
PS–(CNT–Fn)	Spin-coating (PS) by microcontact printing (CNT–Fn)	From tens (~40) to hundreds (~360)	High flexibility, cell adhesiveness and surfaces with tailored morphology	Platforms to direct the cellular organization and engineer the hierarchically assembled tissue structure. Flexible devices for regenerative medicine	98
$(PAH–PSS)_n$PAH–Au–$(PAH–PSS)_n$–PAH	Spin-coating assisted LbL	25–70	E = 30–40 GPa, σ_{max} > 100 MPa and ε_{max} = 2%. Light blue color. Long life, extraordinary sensitivity and unique auto-recovering ability	Although no biomedical application was directly examine, these FsNMs are potential candidates for their use in systems requiring outstanding mechanical and dynamical properties.	4 and 99
PAA–DMLPEI	LbL	<100 (from 2 to 20 bilayers)	Mechanical robustness and pH responsive	Coatings with microbicide properties for airborne and waterborne bacteria	101
DGI	Free-radical polymerization under UV radiation	<5	High mechanical strength and thermal stability. High-density of functional groups exposed to the outer surfaces	Practical applications in the biomedical field depend on the surface post-functionalization	104

[a] E: elastic modulus. L_c: critical load related to the adhesion. σ_{max}: ultimate tensile strength. ε_{max}: ultimate tensile elongation.

This journal is © The Royal Society of Chemistry 2015

Open Access Article. Published on 28 May 2015. Downloaded on 4/2/2026 11:03:23 AM.
This article is licensed under a Creative Commons Attribution 3.0 Unported Licence.

4. Biomedical applications of insulating and electrochemically inactive free-standing nanomembranes

Generally, FsNMs for biomedical applications are made using synthetic or naturally derived polymers. Among the synthetic ones, linear aliphatic polyesters, such as poly(lactic acid) (PLA) and poly(lactic-*co*-glycolic acid) (PLGA), have been extensively chosen since their biodegradation rate and mechanical properties can be easily controlled through variations in their molecular weight.[50] Also, poly(ether ester) copolymers have been successfully employed due to their excellent properties (*e.g.* elasticity, toughness, strength and easy processability), which arise from the combination of both soft and hard segments along their chemical structure.[51] In regard to biopolymers, the most frequently used are collagen and polysaccharides, such as alginate and chitosan, their applications being usually focused in tissue engineering.[52,53]

In the biomedical context, FsNMs need specific requirements such as biocompatibility and, in some cases, biodegradability and/or bioresorbability also need to be met. Furthermore, by successfully controlling the chemical composition and the fabrication process, it is possible to tune and adjust the physicochemical, mechanical, chemical and morphological properties of FsNMs to promote cell–substrate interaction, which is particularly relevant in regenerative medicine (*i.e.* cellular organization can be directly regulated through the cellular microenvironment).[54,55] Their structure and flexibility allow FsNMs to coat the surface of devices that interact with biological systems or, alternatively, FsNMs can be introduced into a needle by aspiration, and then be moved and released/injected into liquid environments (*e.g.* finely positioned on surgical incisions or directly used for wound treatments).

Next sub-sections review the most representative examples of FsNMs made of insulating polymers for advanced biomedical applications. Table 2 summarizes their main characteristics, which are described below organized by polymeric families (namely, polyesters, polysaccharides and other polymeric sources).

4.1. Polyester free-standing nanomembranes

Takeoka and co-workers[56] developed PLA FsNMs (Fig. 4a) with a thickness of 23 ± 5 nm by spin-coating a PLA solution (5 mg mL^{-1}) at 4000 rpm for 20 s onto a poly(vinyl alcohol) (PVA) sacrificial film. The mechanical properties and adhesion strength of the resulting transparent films, which exhibited a flat and uniform surface without cracks, were evaluated using the bulging test and the microme-scratch test, respectively. These PLA-based FsNMs showed a low elastic modulus (1.7 ± 0.1 GPa) and high adhesiveness [the critical load for the detachment of the nanosheet adsorbed onto a SiO_2 substrate was (1.7 ± 0.3) × 10^5 N m^{-1}], which encouraged the analysis of their feasibility as a wound dressing in an *in vivo* experimental gastrostomy model test. The results were extremely positive, showing an excellent sealing efficacy that did not require adhesive agents. Moreover, the incision healed completely without scars and tissue adhesion. In an effort to deeply investigate the possible biomedical application of these PLA FsNMs, their antiadhesive and fixative characteristics were further investigated: an intraperitoneal polypropylene overlaid mesh (IPOM) with PLA nanosheets was placed on an intact peritoneum (Fig. 4b).[57] The results evidenced that PLA FsNMs are feasible to induce adhesion prophylaxis in the IPOM, having a beneficial effect as an atraumatic fixation tool. In addition, it was found that nanosheets do not cause inflammatory reaction, which was attributed to the excellent biocompatibility of PLA.[57]

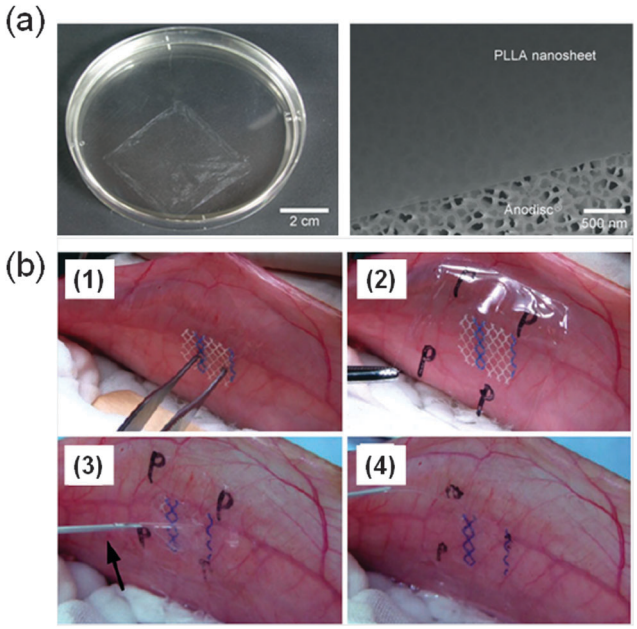

Fig. 4 (a) PLA FsNMs with a thickness of 23 ± 5 nm prepared by Takeoka and co-workers:[56] the macroscopic image of the nanosheet suspended in water (left) and the SEM image of the nanosheet on an anodisc membrane (right). Reproduced with permission.[56] Copyright 2009, Wiley-VCH. (b) Technique of overlaying a PLA FsNM on a large-pore polypropylene mesh for an intraperitoneal onlay mesh (IPOM) without a fixation suture: (1) mesh placed on the peritoneum of a rabbit; (2) overlaying of a PLA FsNM supported by a water soluble PVA sacrificial layer on which the letter "P" is written to distinguish the PLA side; (3) dissolution of the PVA substrate with saline (arrow); and (4) after dissolution of the PVA film, the letter "P" is not visible. Reproduced with permission.[57] Copyright 2011, Springer.

Within this research line, in another study, Takeoka and co-workers[58] tested the feasibility of PLA FsNMs as a wound dressing against burn infections in an *in vivo* mouse model partial-thickness injury. PLA FsNMs tightly adhered onto the burn lesion on the mouse back without any adhesive agents, while adhesion to any opposing tissues/organs was not observed. Moreover, its transparency enabled the visual observation of the wound condition, and thus the infection evolution and the healing process were easily monitored. In addition, PLA FsNMs functioned as a barrier against *Pseudomonas aeruginosa* when it was inoculated on the wound lesion. Therapy with the PLA nanosheet protected against an inflammatory response.[59] Hence, the tested system rendered an effective dressing material for the management of partial-thickness burn wounds.

 This journal is © The Royal Society of Chemistry 2015

Open Access Article. Published on 28 May 2015. Downloaded on 4/2/2026 11:03:23 AM.
This article is licensed under a Creative Commons Attribution 3.0 Unported Licence.

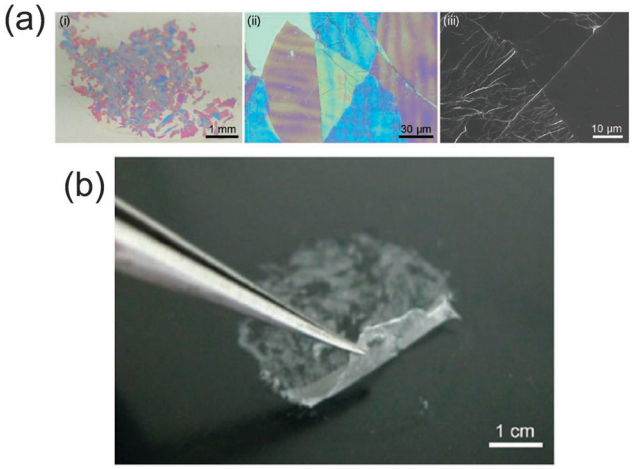

Fig. 5 Patched PLA FsNMs coming from several fragmented nanosheets: (a) macroscopic (i) and microscopic (ii and iii) images of fragmented PLA nanosheets adhered on a SiO_2 substrate using a digital camera, a digital microscope, and a scanning electron microscope, respectively; (b) detachment of fragmented PLA FsNMs from a poly(tetrafluoroethylene) plate. Reproduced with permission.[59] Copyright 2013, Wiley-VCH.

More recently, the same group obtained PLA nanosheets by combining a spin-coating-assisted multi-layering process of PVA and PLA with a peeling step. Therefore, after spin-coating and dissolution of the sacrificial PVA layers between PLA layers in distilled water, a number of PLA FsNMs which corresponded to the number of multi-layering processes of PVA and PLA were obtained.[59] The thickness of the resulting FsNMs, which were transparent and extremely flexible, was determined to be 60 ± 6 nm when spin-coating a PLA solution (10 mg mL^{-1}) at 4000 rpm for 20 s. Later, these nanosheets were fragmented to form a stable suspension, and then reconstructed to form a single continuous film that attached to various interfaces without the need of adhesive agents (Fig. 5). The new patched film was applied as a physical barrier against burn wound infection with *P. aeruginosa*. Both *in vitro* and *in vivo* assays evidenced that the patched film exhibited excellent barrier ability to prevent infection during the treatment of burns for 3 days.

With the aim of designing a novel patch for bone or tendon repair and healing, Pensabene *et al.*[60] studied the biocompatibility, adhesion and proliferation activity of several cell types onto PLA FsNM prepared by spin-coating (2 wt% PLA solution in dichloromethane at 4000 rpm for 20 s using PVA as a sacrificial layer). Their average thickness, which was assessed by AFM, was 320 ± 27 nm, while the elastic modulus, derived from bulge test experiments, was 136 ± 44 MPa. Both immortalized cell lines and primary cell lines cultured on those FsNMs exhibited good morphological and metabolic features and the ability to fully differentiate. In addition to the *in vitro* assays, the adhesion of such PLA FsNMs to ligament and femur was evidenced under *ex vivo* conditions using a rabbit model. Moreover, their short- and medium-term biocompatibility were evaluated using C2C12 cultured cells.[61] The results evidenced early differentiation with the fusion of cells into firmly adherent myotubes, proving that such flexible nanofilms behaved as good bioactive matrices for cell anchoring, spreading and proliferation.

The effect of an underlying substrate on the interaction between cells and PLA FsNMs was recently investigated.[62] For this purpose, polyester-based nanosheets (with thickness values from 29 ± 1 nm to 703 ± 4.4 nm, depending on the PLA concentration during the spin-coating process) were also fabricated by spin-coating and PVA acted as the sacrificial layer. After releasing PLA FsNMs in a liquid environment, they were collected on a stainless steel mesh (PLA-mesh), and subsequently used for cell adhesion studies using rat cardiomyocyte cells (H9c2). The results were compared to the ones obtained on a control interface: SiO_2 substrates coated with an ultra-thin layer of PLA (PLA-substrate). Although topological and mechanical properties of PLA FsNMs did not influence the cell viability after 24 h of culturing, cells did geometrically sense the stiffness of the underlying material, thus affecting the adhesion geometry. Briefly, the PLA-mesh induced an anisotropic adhesion of H9c2 cells along the metal wire, while H9c2 cells on the PLA-substrate adhered isotropically, independent of the nanosheet thickness. Accordingly, cells distinguished the increase in the nanosheet stiffness and preferentially adhered onto the rigid interface. Interestingly, cellular anisotropy decreased by increasing the thickness of the PLA FsNM deposited onto the mesh because the nanosheet stiffness was more homogeneous throughout the surface. Considering the huge difference between the Young's modulus of PLA FsNMs (from 3.5 ± 1.3 to 7–10 GPa depending on the thickness) and the metal substrate (hundreds of GPa), it was concluded that cell adhesion was mechanically regulated by the stiffness of the underlying substrate when the thickness of the PLA FsNM was in the order of tens of nanometers.

PLA FsNMs have also been modified and/or functionalized by means of collagen deposition, magnetic particle entrapment and drug loading. In a recent study, Niwa *et al.*[63] prepared PLA nanosheets by modifying only one surface with collagen to endow different discrete functions to each side of the nanosheet: anti-adhesive and pro-healing properties. For this purpose, PLA FsNMs were prepared by spin-coating using conditions similar to those previously described (thickness: 59.5 ± 9.5 nm). A collagen layer was subsequently deposited on the surface following two approaches: solvent casting or spin-coating. The latter strategy resulted in an ultra-thin collagen coating (thickness of 5–10 nm), which is more homogeneous and hydrophilic than that obtained by solvent casting exhibiting a thickness of ~120 nm. The disorganized collagen fibrils formed on PLA nanosheets when covered using the spin-coated method induced a hydrophilic microenvironment that improved cell adhesion and spreading, in comparison to that obtained by solvent casting. Besides, fine networks of actin filaments were clearly identified in cells cultured on the former biointerface, as opposed to the latter system.

As a first step to develop remotely controlled and manipulated magnetic FsNMs, Taccola *et al.*[64] embedded superparamagnetic iron oxide nanoparticles (SPIONs) into PLA nanosheets

Open Access Article. Published on 28 May 2015. Downloaded on 4/2/2026 11:03:23 AM.
This article is licensed under a Creative Commons Attribution 3.0 Unported Licence.

by spin-coating (5–20 mg mL^{-1} of PLA solution in chloroform and 1–15 mg mL^{-1} of SPION colloidal solution at 3000 rpm for 20 s using a PVA sacrificial layer). Magnetic composites were coloured with different degrees of intensity depending on the nanoparticle load, and the inclusion of SPIONs in the polymeric matrix did not alter their magnetic behaviour, yielding FsNMs with high saturation magnetization and magnetic susceptibility. For nanosheets with a high concentration of SPIONs, the magnetic response increased because of the formation of clusters, albeit their presence did not alter the integrity and stability of the FsNM. The results were good enough to promote further investigation in this area, suggesting that controllable supports with magnetic properties could be fabricated in a near future for biomedical applications.

FsNMs with unidirectional drug delivery ability have the potential to improve therapeutic efficacy, while minimizing undesirable side effects. In this sense, Sun and co-workers[65] fabricated robust and flexible FsNMs by sandwiching drug-containing polyelectrolyte multilayer films between a capping and a barrier layer of PLGA. The drug-containing films were prepared by the LbL assembly of chemically cross-linked poly(allylamine hydrochloride)–dextran (PAH–D) microgel and hyaluronic acid (HA), which can load methotrexate (MTX), a negatively charged cancer-inhibiting drug. The PLGA barrier layer, which was obtained by spin-coating, prevents MTX release, and the PLGA capping layer regulates the unidirectional MTX release kinetics in a precisely controlled manner. *In vitro* cancer treatments evidenced that MTX released from the FsNM preferentially inhibited the proliferation of HeLa cells. The versatility of LbL assembled polymeric films as drug carriers allows the loading of a wide variety of drugs and bioactive agents. Thus, the design of highly efficient unidirectional drug-delivery systems with minimum side effects on normal tissues has great potential for clinical applications.

Finally, Okamura *et al.*[66] prepared disk-shaped PLGA nanosheets and modified their surfaces with dodecapeptide H12 (HLGGAKQAGDV), which is a fibrinogen γ-chain carboxy-terminal sequence (γ400–411) that specifically recognizes the active form of glycoprotein IIb/IIIa on activated platelets. Under flow conditions, H12-PLGA FsNMs were found to interact with activated platelets on a collagen surface faster than H12-PLGA microparticles did. In addition, only FsNMs induced 2D spreading of platelet thrombi on collagen-immobilized plates. These results suggested that PGLA FsNMs might be a suitable candidate as novel platelet substitutes and, also, an alternative to human platelet concentrates infused to treat bleeding in patients with severe thrombocytopenia.[66]

4.2. Polysaccharide free-standing nanomembranes

Polysaccharides are a class of biological macromolecules that participate in a wide range of biochemical and biomechanical functions. Because of their unique properties, these biopolymers are currently playing an important role in materials science. The structure and function of polysaccharides, and their nanoscale assembly for biomedical materials were recently reviewed by Boddohi and Kipper.[67] However, this section will draw the attention to those studies that used polysaccharides as the main polymeric source to develop and design FsNMs. As in the previous section, biomedical applications and promising results will be highlighted.

In 2007, Fujie, Okamura and Takeoka[68] constructed what they called a "nano-adhesive plaster", a multilayered FsNM (thickness: 30.2 ± 4.3 nm) made of chitosan and sodium alginate (Na-alginate) that was deposited onto a PVA–silicone rubber substrate using the spin-coating assisted LbL approach. More specifically, the layers of each polyelectrolyte were spin-coated on the silicone rubber (millimetre scale thickness: 1.0 mm) previously covered with a sacrificial PVA layer (microscale thickness: 1.2 μm). As a result, the nano-adhesive plaster was formed by the superposition of three different types of free-standing sheets (Fig. 6a). Chitosan and Na-alginate contain amino and carboxylic groups, respectively, as cationic and anionic polyelectrolytes at ambient pH, which enormously facilitated their assembly in the FsNM. The elastic modulus, which was determined by the bulge test, was found to be 1.3 GPa. The good adhesiveness and flexibility of the nano-adhesive plaster were evidenced by transferring it, after modification with a luminescent pigment for ease of visibility, not only onto the skin of a human arm[68] (Fig. 6b–d) but also onto a tissue (rat cecum) surface.[69] In a subsequent study, the same group proved the potential biomedical application of this adhesive, which is a robust and flexible nano-adhesive plaster made of chitosan and Na-alginate in a surgical intervention.[70] Thus, a FsNM with a thickness of 75 nm repaired an *in vivo* visceral pleura defect induced on beagle dogs without any loss in the respiratory function and without significant inflammatory response. In addition, the influence of the thickness on the mechanical properties of

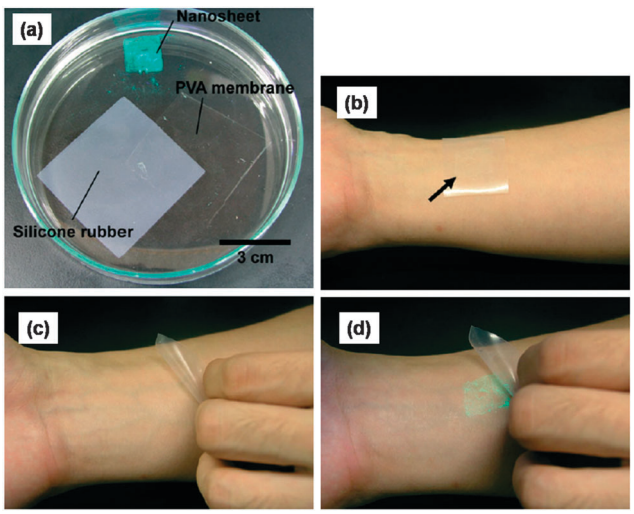

Fig. 6 (a) Elements used to fabricate the nano-adhesive plaster floating in acetone: silicone rubber (substrate), PVA sheets (sacrifial layer) and polyssacharide FsNMs photographed in the dark (the polysaccharide FsNM was modified with the luminescent pigment for easy visibility). Nano-adhesive plasters on the human skin (b) before the polysaccharide FsNM was released from the silicone rubber and (c) after release from such a substrate. (d) Same image as (c) except that it was captured in the dark. Reproduced with permission.[68] Copyright 2007, Wiley-VCH.

This journal is © The Royal Society of Chemistry 2015

Open Access Article. Published on 28 May 2015. Downloaded on 4/2/2026 11:03:23 AM.
This article is licensed under a Creative Commons Attribution 3.0 Unported Licence.

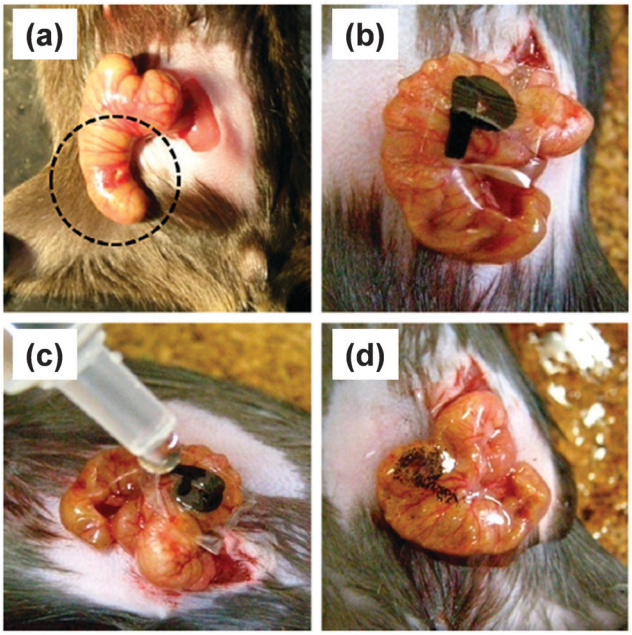

Fig. 7 FsNMs made of chytosan and Na-alginate were applied to a murine model of cecal puncture: (a) cecal defect site punctured with a needle (dashed line circle showing an actual puncture site); (b) sealing with the polysaccharide nanosheet supported by a sacrifial PVA film, in which the letter "P" was written; (c) dissolution of the PVA film with saline water solution; and (d) after dissolution of the sacrificial layer, the letter "P" is not visible. Reproduced with permission.[71] Copyright 2010, Elsevier.

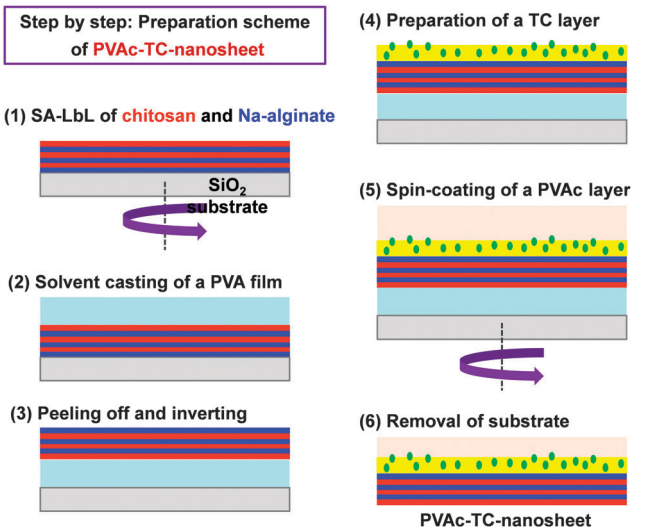

Fig. 8 Preparative scheme for tetracycline (TC) loaded polysaccharide nanosheets made of chitosan and Na-alginate using the spin-coating assisted LbL technique (SA-LbL).

polysaccharide FsNMs was demonstrated, which enabled an easy modulation of the nanosheet features.

Besides, the therapeutic effect of the nano-adhesive plaster on the murine cecal puncture was evaluated (Fig. 7).[71] The sealing effect of the multilayered chitosan and Na-alginate-based FsNM inhibited effectively the bacterial infection, and increased the survival rate of the individuals. Interestingly, the treatment with the polysaccharide nanosheet provoked less inflammatory response than the suture.[71] Despite the promising results, a small percentage of bacteria was able to pass through the FsNM. To overcome this aspect, an antibiotic-loaded polysaccharide nanosheet was developed.[72] In this new approach, an antibiotic (tetracycline, abbreviated as TC) was sandwiched between a new PVA layer (named PVAc in Fig. 8), which acted as a protector, and the LbL assembled polysaccharide platform (total thickness: 177 nm). The resulting FsNM, which comprehended three functional layers (Fig. 8), exhibited an important anti-microbial effect and a relatively low inflammatory tissue response.[72] As a consequence, *in vivo* studies using overlapping therapy with these new PVA–TC–polysaccharide FsNMs showed a significant increase in mouse survival after cecal puncture. Later research evidenced that TC-loaded chitosan and Na-alginate multilayered FsNMs exhibited a potential antibacterial activity when covering mice dorsal skin artificially burnt and infected with *P. aeruginosa*.[73] All mice treated with the TC-loaded polysaccharide FsNM survived, whereas mice treated with TC-unloaded nanosheets and mice left untreated displayed increased rates of mortality due to bacterial infection. Moreover, TC-loaded FsNMs prevented not only local inflammation but also systematic inflammation.

Hagisawa *et al.*[74] described a novel therapy in which the overlapping of several chitosan–Na-alginate FsNMs with a thickness of 75 nm (*i.e.* multioverlapping therapy) sealed and stopped a massive venous hemorrhage in rabbits. Before *in vivo* tests, the mechanical durability of the nanosheets and their hydrostatic pressure resistance were evaluated. Four pieces of overlapping nanosheets were able to stand 80 ± 6 mm Hg of pressure. In regard to their degradability, polysaccharide nanosheets experience a decrease in their thickness under degradation conditions (phosphate-buffered saline, PBS, at 37 °C). Nevertheless, they retained more than 70% of the thickness after seven days. Positively, after one month, no inflammatory tissue reaction was detected around the FsNM attachment and findings revealed a complete wound healing. The multioverlapping therapy would represent a great advantage for surgical operation, especially in trauma patients with bleeding from large veins.

Otani *et al.*[75] have reported the therapeutic use of bilayered polysaccharide FsNMs made of chitosan and Na alginate as an arachnoid plaster in a microneurosurgery environment because of their semi-absorbent and potent physical adhesive strength features. These authors observed that the application of overlapping FsNMs without using chemical bonding agents completely avoided cerebrospinal fluid leakages in the cerebral cortex. There was evidence of a relationship between the number of overlaid nanosheets and the reinforcement effect: the more the layers displayed, the more they improved. Besides, after six months, no inflammatory infiltration was detected.

In addition to chitosan and Na-alginate, proteoglycan HA has also been used to fabricate polysaccharide FsNMs. For instance, Fujie *et al.*[76] prepared multilayered nanosheets of HA and collagen on a water-soluble sacrificial supporting substrate using the LbL assembly method. The thickness of these FsNMs was found to grow exponentially with the number of HA and

Open Access Article. Published on 28 May 2015. Downloaded on 4/2/2026 11:03:23 AM.
This article is licensed under a Creative Commons Attribution 3.0 Unported Licence.

collagen layers. This was attributed to the fact that the amount of HA adsorbed in the LbL structure is less than that of collagen.[77] Therefore, the polyion pairs mediated by the electrostatic interaction between collagen and HA molecules induced nonlinear growth in the LbL system. The mechanical properties of these FsNMs, as determined by the bulge test, were found to depend on the fibrous or non-fibrous structure of collagen layers. Thus, the elastic modulus of nanosheets made of non-fibrous collagen and a high content of HA (thickness: 62 ± 7 nm) was 4.3 ± 0.6 GPa, which is a value comparably smaller than that of the previously reported chitosan/Na-alginate nanosheet (9.6 GPa for a thickness of 75 nm[70]). This low elastic modulus was attributed to the hydrophilic and moisture-sensitive nature of HA molecules. In contrast, the elastic modulus of FsNMs made of fibrous collagen (thickness: 42 ± 4), which had a low content of HA, increased to 12.5 ± 1.5 GPa, thus evidencing a greater mechanical durability. Collagen structures in bone and skin have an elastic modulus of 17.2 and 4 GPa, respectively. Therefore, FsNMs made of HA and fibrous or non-fibrous collagen efficiently imitate the mechanical properties of these tissues. Consistently, FsNMs made of non-fibrous collagen exhibited a surface with softer elastic properties than those observed in FsNMs with fibrous collagen. Besides, cell adhesion studies using NIH-3T3 cells showed that HA/non-fibrous collagen FsNMs gave lower cell adhesive elongation in comparison to nanosheets with fibrous collagen and a low content of HA. On the basis of this study, the authors concluded that cell adhesive properties can be tuned by changing the structural components of the nanosheets (*i.e.* the content of polysaccharide and collagen fibrils),[76] thus opening a new door for the production of novel engineered scaffolds for regenerative medicine as well as cell biology.

An innovative and audacious strategy has been recently reported by Chen *et al.*[78] who prepared cell–polymeric nanocomposites for the fabrication of FsNMs lined with cells (Fig. 9). First, poly(*N*-isopropylacrylamide) (PNIPAM), a temperature-responsive polymer, was grafted onto glass-slides. After this, cells were cultured on the resulting hydrophobic layer. Once 80–90% cell confluence was achieved, the LbL process was conducted on the surface of the cell sheet. However, gelatin, a natural biocompatible polyelectrolyte, was previously deposited as the cell-contacting layer to maintain a high cell viability during the deposition process.[79,80] Thus, this gelatin layer is of great importance during the LbL self-assembly step on the cell-sheet surface.[79,80] Specifically, three alternating charged polysaccharide bilayers of chitosan and Na-alginate, (chitosan–Na-alginate)$_3$, were assembled onto the gelatin-coated cells cultured on the PNIPAM-grafted surfaces. The deposition of gelatin, chitosan and Na-alginate layers, which are extracellular matrix (ECM) related components, on the cell sheet resulted in a cell adhesive surface that efficiently interacted with cells.[81] The free standing cell–gelatin–(chitosan–Na-alginate)$_3$ film was peeled off from the PNIPAM-grafted surface upon temperature changes. By this strategy, the assembly of cell sheets with ultra-thin ECM components to form FsNMs can be potentially used to fabricate complex artificial soft tissues to substitute some elements in native tissues.

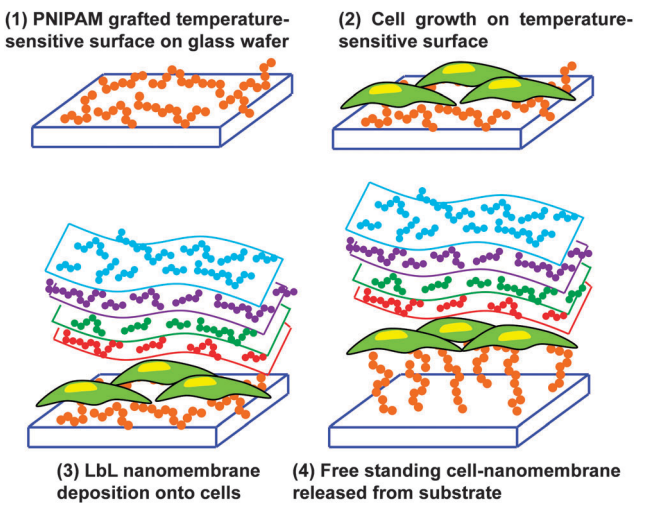

Fig. 9 Schematic illustration of fabrication of cell–gelatin–(chitosan–Na-alginate)$_3$ FsNMs.

4.3. Other polymeric sources for free-standing nanomembranes

Poly(ethylene oxide) (PEO) is a thermoplastic biocompatible material widely used in biomedical applications, for example scaffolds, drug delivery systems and sensor devices.[82–84] To extend their application list, the LbL technique was used to fabricate FsNMs made of PEO.[85] This was achieved by creating solid-state hydrogen bonded assemblies that allowed the incorporation of stable interdigitated layers of PEO and poly(acrylic acid) (PAA) at the nanometer length scale (the thickness of each PEO–PAA bilayer was 80 nm). Free-standing films containing 100 bilayers were transparent, smooth to touch and exhibited elastomeric properties during handling. Although these were not explicitly proved with experiments, Lutkenhaus *et al.*[85] suggested many biomedical applications for these hydrogen bonded assemblies, for example biosubstrates, drug delivery devices and pH-sensitive sensors.

Ono and Decher[86] reported the use of pH-responsive self-standing polyelectrolyte multilayer membranes, which were fabricated by spraying polymer solutions, for biomedical applications. Concretely, a silicon wafer substrate was covered by a sacrificial multilayered film made of PAA and poly(ethylene glycol) (PEG), which disintegrated by a pH change releasing a target membrane. In that work, the released membrane consisted of a simple polyelectrolyte multilayered film of poly(allylamine hydrochloride) (PAH) and poly(sodium-4-styrenesulfonate) (PSS), which was initially constructed on the top of the PAA–PEG pH-responsive film. The pH response mechanism is based on the alteration of the hydrogen bonds established between PAA and PEG when the carboxylic acid groups present in PAA transform into carboxylate ions. From a biomedical point of view, the advantages of the PAA–PEG pH-responsive film, which was obtained with thickness values ranging from 55 to several hundreds of nanometers and areas of a few square centimetres, rely on the fact that PAA and PEG are biocompatible,

 This journal is © The Royal Society of Chemistry 2015

Open Access Article. Published on 28 May 2015. Downloaded on 4/2/2026 11:03:23 AM.
This article is licensed under a Creative Commons Attribution 3.0 Unported Licence.

biotolerated or bioinert. Accordingly, their release would not lead to adverse effects in the bioenvironment, and thus could be used in therapeutic devices and aids.

In another example, the preparation of PEG-terminal FsNMs was based on the extensive cross-linking of aromatic 4′-nitro-1,1′-biphenol-4-thiol (NBPT) self-assembled monolayers (SAMs) deposited onto a gold support by exposure to low energy electrons, thus resulting in a mechanical and thermally stable monolayer.[87] Simultaneously, the terminal nitro groups of the NBPT molecules were converted to reactive amine moieties to which epoxy functionalized PEG chains were subsequently coupled. As a result, these films exhibited protein repelling properties, which in turn ensure the lack of protein denaturation when they are used as a support in transmission electron microscopy studies.[87]

Meyerbröker and Zharnikov developed highly elastic, hydrophilic and ultra-thin membranes consisting entirely of PEG.[88] This was achieved by preparing an ultra-thin stable PEG-hydrogel precursor film composed of a mixture of epoxy- and amine-terminated PEG moieties, which was deposited onto a supported sacrificial layer (*i.e.* a 100 nm gold film evaporated onto a silicon substrate). Then, the complementary terminal groups underwent chemical crosslinking.[89] Afterwards, the PEG–gold bilayer was separated from the silicon support and the sacrificial layer was dissolved releasing the PEG FsNM, which could be transferred onto a grid or any other arbitrary substrate. These nanosheets exhibited sufficient mechanical stability, and also high flexibility (extraordinary low Young's modulus of only $\sim$2 MPa). Such a behavior is characteristic of elastomers,[90] and it was never observed before in nanomembranes. Indeed, the only analogous systems are polyisoprene and polyisobutene nanomembranes, which are not biocompatible, prepared using Langmuir–Blodgett technology.[17] On the basis of their properties, PEG nanosheets are potentially useful as a highly sensitive support and a sensor element for biological samples.

In another study, porous multilayered films of PAH and PAA were prepared using the LbL dipping technique, nanopores being subsequently created using a pH treatment.[11] The porosity induced by pH adjustment resulted in a significant increase in the thickness. For example, the thickness of films made of 8 PAH–PAA bilayers before and after the creation of nanopores was 101 and 253 nm, respectively. Ketoprofen and cytochalasin D, which represent different types of drugs that can be entrapped in these films, were successfully loaded and showed zero order release kinetics over a long period of time. The amount of drug loaded and released could be tuned by varying the number of bilayers in the porous regions of the films, whereas variations of the pore size controlled the release flux of the given drug. On the other hand, sheet- and tube-like FsNMs of PAA–PAH were prepared by exfoliating PAA–PAH multilayered films from substrates in an aqueous acid solution containing Cu^{2+}.[91] Initially, multilayered films were prepared by LbL deposition onto silicon wafers, quartz or glass tube substrates. Their ion-triggered exfoliation was achieved by breaking the electrostatic interactions between the PAA layer and the underlying substrate. However, it should be noted that, although PAA–PAH bilayers were nanometric, ion-triggered exfoliation was applied to films with 15 bilayers of submicrometric thickness ($\sim$0.8 μm) and, therefore, these cannot be considered as nanomembranes. The developed technology was proposed for the fabrication of small-caliber artificial blood vessels.

Gui *et al.*[92] fabricated LbL multilayer films made of poly(diallyldimethylammonium) (PDDA) and poly(4-vinylpyridine propylsulfobetaine) (P4VPPS), a zwitterionic polysulfobetaine, in an acid aqueous solution at pH 2 with 0.5 M NaCl. The average growth rate was estimated to be $\sim$29.0 nm per PDDA–P4VPPS bilayer. These films were pH-dependent, thus disintegrating in alkali aqueous solution, especially at pH $\geq$ 12, which suggested a potential application as sacrificial layers for the release of other polymeric films. This was proved by depositing a multilayered film of PDDA and poly(sodium 4-styrenesulfonate) (PSS) on the top of a 10-bilayered PDDA–P4VPPS sacrificial film. After treatment with alkali aqueous solution at pH 12, the PDDA–PSS film was released maintaining its integrity in air. Previously, Dubas *et al.*[93] had reported the fabrication of PDDA–PSS FsNMs using PDDA–PAA LbL multilayer films as sacrificial layers.

Kohri *et al.*[94] presented a new approach for the fabrication of smooth and stable FsNMs composed of a polymer brush, poly(2-hydroxyethyl methacrylate) (PHEMA), supported on an ultra-thin (*i.e.* $\sim$6 nm) colourless polydopamine (PDA) layer. This was achieved through the surface-initiated atom radical polymerization (ATRP) of 2-hydroxyethyl methacrylate (HEMA) on the PDA layer, which resulted in optically transparent and colourless free-standing PHEMA brush films with a tailored thickness of 16–75 nm. Prior to this process, the PDA ultra-thin film was placed onto a silicon or glass substrate covered by a cellulose acetate sacrificial layer (thickness: $\sim$115 nm). The scheme of the synthetic design is displayed in Fig. 10. Although no application was explicitly tested, the authors suggested that PHEMA FsNMs can be used as multi-stimuli responsive sensors after functionalizing their surface.[94]

Surface-functionalized FsNMs were produced grafting poly(2-methacryloyloxyethyl phosphorylcholine) (PMPC) brushes by the ATRP of 2-methacryloyloxyethyl phosphorylcholine (MPC) on nanosheets made of PAH, PAA and PS, which were prepared by the spin-coating assisted LbL technique (a thickness of 85 ± 2 nm).[95] The properties of PMPC-nanosheets (physiological stability, surface wettability and anti-biofouling response) were regulated by several parameters, such as the thermal crosslinking of the FsNM, the grafted amount of MPC and the thickness of PMPC brushes (*ca.* 11 nm). PMCP-nanosheets were easily peeled, transferred using tweezers with the aid of a water-soluble PVA sacrificial layer, cut into any shape using scissors, and patterned using a needle. Nanosheets patched on cell culture substrates exhibited anti-biofouling properties such as anti-coagulant behaviour of human blood cells as well as the potential to microscopically pattern murine fibroblasts cells. The overall results provided an important physicochemical insight into the remarkable biological response of surface-functionalized nanosheets, which represent not only a powerful tool for biomedical applications but also an alternative to conventional micropatterned techniques used in bionanotechnology.

Open Access Article. Published on 28 May 2015. Downloaded on 4/2/2026 11:03:23 AM.
This article is licensed under a Creative Commons Attribution 3.0 Unported Licence.

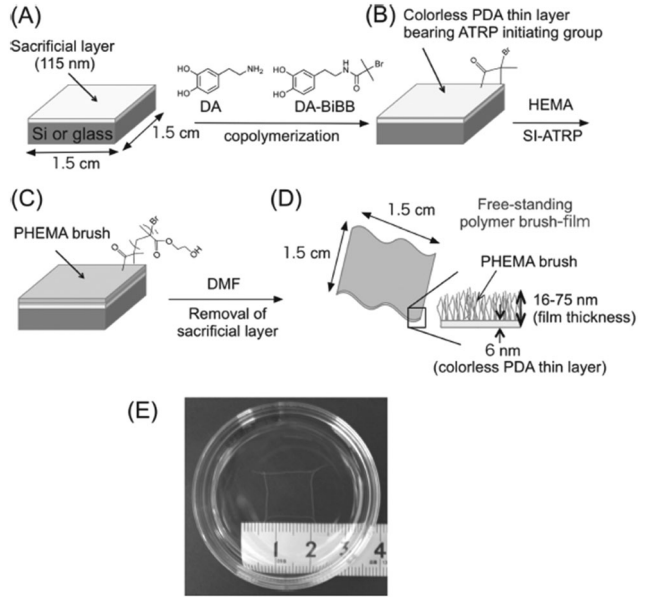

Fig. 10 Schematic representation of the preparation of a free-standing polymer brush film based on a colorless PDA thin layer: (A) spin-coating of a sacrificial cellulose acetate layer onto the silicon plate; (B) creation of a colorless PDA thin layer containing an ATRP-initiating group; (C) construction of polymer brushes on the substrate by surface initiating ATRP; (D) recovery of polymer brush film based on a PDA layer by the dissolution of the cellulose acetate layer in DMF; and (E) photographic image of the obtained free-standing PHEMA brush film floating in dimethylformamide. Reproduced with permission.[94] Copyright 2013, Wiley-VCH.

Fujie *et al.*[96] developed spatio-selective cell culture environments by inkjet printing bio-patterns onto FsNMs composed of poly(methyl methacrylate) (PMMA). The thickness of the nanosheets, which were prepared by spin-coating, was *ca.* 200 nm. Interestingly, several cell adhesion promoters, such as poly-(L-lysine) modified with fluorescein isothiocyanate, were micropatterned on the FsNM surface and, subsequently, functionalized with fibronectin by electrostatic interaction. The high flexibility of PMMA FsNMs made it an ideal substrate for cell adhesion and spreading. *In vitro* assays showed the selective deposition of C2C12 skeletal muscle myoblasts following these patterns. Accordingly, the protein micropatterned FsNM system was proposed as an interesting tool for cell-directed culture in muscular tissue engineering.

PMMA was also employed for the preparation of FsNMs displaying the phase separation morphology. This was achieved by spin-coating a polymer mixture solution of PMMA and polystyrene (PS) onto a PVA-coated substrate.[97] Due to the intrinsic immiscibility of PMMA and PS, rapid quenching during the spin-coating process induced their phase separation. In order to obtain porous nanosheets, PS regions were dissolved by immersing the PMMA–PS FsNM into cyclohexane. The thickness of these films, which ranged from 38.8 ± 1.1 to 110.2 ± 2.0 nm, and the diameter of the pore, which varied between 64.4 ± 9.3 and 187.2 ± 33.9 nm, were controlled through the PMMA : PS ratio and the spin-coating conditions. Furthermore, the authors demonstrated that when the thickness of the ultra-thin films is comparable to the dimensional scale of the phase separation domains, it is possible to prepare perforated FsNMs with nanopores in the range of tens of nanometers.[97] The availability of these perforated FsNMs is proposed to be of immense value in many biomedical applications, for example cell culture devices, high flux biosensors and drug delivery systems.

Flexible PS FsNMs for directing cellular organization were prepared by Fujie *et al.*[98] by combining spin-coating and microcontact printing methodologies. The PS nanosheet thickness, which ranged from tens to hundreds of nanometers, was controlled through the concentration of the polymer solution used during the spin-coating process. In this work, the sacrificial layer was made of PNIPAM. After hydrophilization of the PS nanosheet surface, a composite made of multi-walled carbon nanotubes and fibronectin (CNT–Fn) was micropatterned on the FsNM using poly(dimethylsiloxane) (PDMS) molds with microscopic groove-ridge features (width and separation of ~50 μm). Then, unpatterned regions were rendered cytophobicity by Pluronic F-127 to promote initial cell alignment. As a result, the CNT–Fn nanocomposite was homogeneously distributed onto the flexible PS nanomembrane (Fig. 11a). Nanomechanical mapping revealed the high flexibility of these engineered nanomembranes by simply decreasing the film

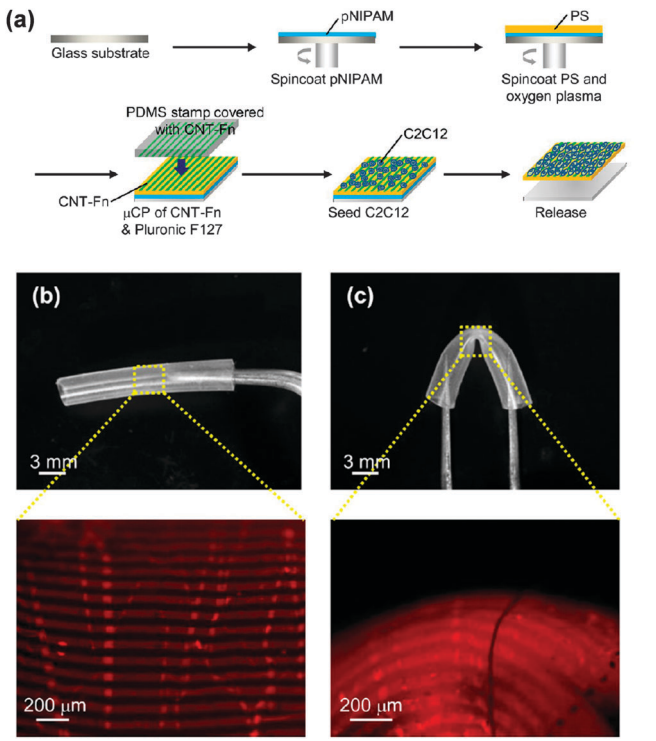

Fig. 11 (a) Schematic of the preparation of PS nanomembranes with micropatterned CNT–Fn nanocomposites and aligned C2C12 myoblasts. Macroscopic and magnified fluorescence images of the nanomembranes (40 nm thick) wrapping a silicone tube (3 mm diameter) (b) before and (c) after bending the tube. The micropatterns (rhodamine labeled fibronectin) were flexible and adhered to the curvature of the tube in the bending state. Reproduced with permission.[98] Copyright 2013, American Chemical Society.

This journal is © The Royal Society of Chemistry 2015

Open Access Article. Published on 28 May 2015. Downloaded on 4/2/2026 11:03:23 AM.
This article is licensed under a Creative Commons Attribution 3.0 Unported Licence.

thickness. This flexibility is illustrated in Fig. 11b and c, which display the bending of a silicone tube wrapped with 40 nm thick PS/CNT–Fn FsNMs. Therefore, the combination of their outstanding features (*i.e.* high flexibility, cell adhesiveness and surfaces with tailored morphology) suggests that such systems recreate the properties of the extracellular matrix (ECM). Cell-adhesive micropatterns facilitated the alignment of C2C12 skeletal myoblasts, while CNTs enhanced the cellular elongation and differentiation to generate functional myofibers.

In an earlier study, Tsukruk and co-workers[4,99] prepared hybrid organic–inorganic FsNMs with extraordinary sensitivity and unique auto-recovering ability. These nanosheets (a thickness of 25–70 nm) were prepared by spin-assisted LbL assembly of PAH and PSS on a sacrificial substrate. The most innovative aspect of these FsNMs is the intercalation of a central layer containing gold nanoparticles (a diameter of 12.7 nm) sandwiched between PAH–PSS bilayers. Thus, the general formula of these nanosheets can be described as: $(PAH–PSS)_n$PAH–Au–$(PAH–PSS)_n$–PAH, where n was varied between 3 and 11. The thickness of the system with a gold central layer was $\sim$20 nm higher than that of films without gold nanoparticles, independent of n. The mechanical properties of these hybrid FsNMs (an elastic modulus of 30–40 GPa, an ultimate strain of about 2% and an ultimate tensile strength higher than 100 MPa) were found to surpass those reported for a much thicker (*i.e.* submicrometer scale) nanoparticle-containing free-standing LbL films.[99] Moreover, the overall examined properties suggested a wide variety of prospective applications,[4] those related to the development of chemical and temperature micro-array sensors being particularly relevant in the biomedical field.

Metallic nanoparticles were also used to fabricate a superhydrophobic/hydrophilic asymmetric FsNM using the LbL approach on a Teflon substrate.[100] In this case, the layer assembly was achieved between a poly(ethyleneimine)–Ag^+ complex (PEI–Ag) at pH 9 and PAA at pH 3.2. The incorporated silver ions were reduced to silver nanoparticles during the thermal treatment applied to promote the cross-linking by imide bond formation. As a result, silver loaded films displayed asymmetric wettability: the top surface was superhydrophobic, while the bottom one was hydrophilic. On the one hand, the superhydrophobic side limited the bacterial adhesion and exhibited self-cleaning properties; on the other hand, the hydrophilic side delivered bactericidal silver ions. These silver-functionalized hybrid films can have great potential in open wound patches or in the barrier, separation, transportation or drug delivery fields, although exceeding the nanoscale (thickness ranging between 2 and 20 μm, depending on the number of layers). This aspect was overcome by Hammond and coworkers,[101] who designed contact-killing ionically cross-linked LbL ultra-thin films using *N*,*N*-dodecyl, methyl-polyethylenimine (DMLPEI), which has microbicidal activity, layered with PAA (thickness $<$ 100 nm for films with a number of bilayers ranging from 2 to 20). A pH treatment was applied during the assembly process to rearrange the microbicidal polycation chains. Thus, at acid pH, the amount of positive charges on the surface available to interact with the bacterial cell membrane is higher than that at neutral pH. Consistently, films as thin as 10 nm made at pH 3 were more lethal to both airborne and waterborne bacteria than films made at pH 7.

Baxamusa *et al.*[102] proposed the fabrication of FsNMs without using any sacrificial layer for their release from the substrate. More specifically, these authors proposed the direct delamination of ultra-thin films made of poly(vinyl formal) (PVF) resin, PS or PMMA. Delamination of a thin film from its substrate spontaneously occurs when the strain energy (G_v) in the film exceeds the interfacial energy resisting separation (γ). In practice, this occurs when the film thickness (L) satisfies the following condition:[103]

$$L > 2\frac{1+\upsilon_f\gamma}{1-\upsilon_f E\varepsilon^2} \quad (1)$$

where υ_f is Poisson's ratio of the film, γ is the difference in interfacial energy between the laminated and delaminated state, E is the Young's modulus of the film, and ε is the strain mismatch between the film and the substrate. Delamination and capture on wire supports of extraordinarily thin and large polymeric thin films have been enhanced by decreasing the interfacial energy between the film and its deposition substrate through electrostatic adsorption of a cationic polyelectrolyte. By this procedure and using polydiallyldimethylammonium chloride (PDAC) as a polyelectrolyte, the minimum delaminated film thickness for PVF, PS and PMMA was found to be 8, 12 and 15 nm, respectively. The characteristics of this methodology, which can be extrapolated to many types of polymers, make the fabrication of FsNMs for biomedical applications a potential scalable process.

Lastly, extraordinarily thin FsNMs (thickness $<$ 5 nm) were obtained by spatially confined polymerization of a unique and elaborate 2D supramolecular system composed of two liquid-crystalline lamellar bilayer membranes made of self-assembled nonionic surfactant, dodecylglyceryl itaconate (DGI), which was

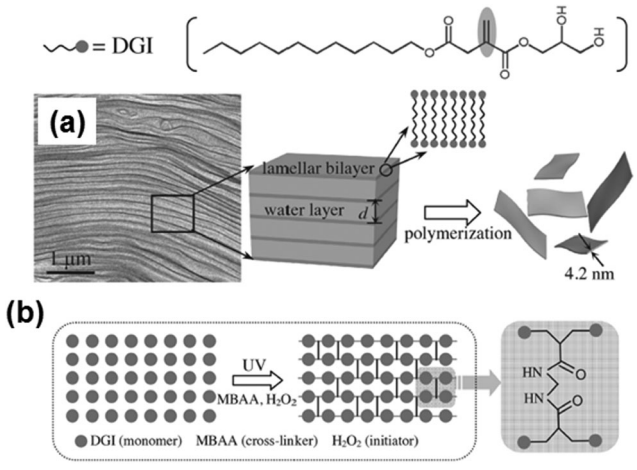

Fig. 12 Schematic illustration for the formation of free-standing, single-bilayer-thick polymeric nanosheets derived from DGI: (a) freeze-fracture electron microscopy image of the DGI system, and (b) top-view schematic showing cross-linking between DGI along one lamellar plane. Reproduced with permission.[104] Copyright 2014, Wiley-VCH.

Open Access Article. Published on 28 May 2015. Downloaded on 4/2/2026 11:03:23 AM.
This article is licensed under a Creative Commons Attribution 3.0 Unported Licence.

sandwiched by a water layer (Fig. 12).[104] Nanosheets are achieved using a simple free-radical polymerization under UV radiation with high yield and in large quantity. The covalently bonded two-molecular-thick sheets exhibited high mechanical strength and thermal stability. Moreover, an important characteristic of these ultra-thin sheets is the high-density of functional groups exposed to the outer surfaces. Post-functionalization of the hydroxyl groups at the head of DGI located on the outer surfaces of these nanomembranes opens the door to many practical applications in the biomedical field.

5. Biomedical applications of free-standing nanomembranes with electroactive conducting polymers

Human body tissues, such as neural, cardiac or skeletal muscle ones, respond to electrical and electrochemical stimuli, signals being able to regulate cell growth and behaviour. However, conventional biomaterials do not result in appropriate bio-interfaces to conduct electrical and/or electrochemical stimulation since they lack both electrical conductivity and electrochemical activity. In order to overcome this drawback, ECPs have been used as biocompatible materials which can support cell adhesion, migration and proliferation.[105] Their properties are of great potential since they can be used to electrically stimulate local tissue,[106–109] exchange ions reversibly with cells, thus promoting adhesion and proliferations of these living systems,[41,110,111] fabricate electronic devices (*e.g.* biocapacitors and biobatteries) that can be implanted in the organism,[112] act as time controlled drug- or bactericidal-release devices,[113,114] detect biomolecules,[115–117] recognize specific fragments of DNA,[118,119] *etc.* Recently, Llorens *et al.*[120] reviewed the advancements in the preparation of structures (*i.e.* essentially fibrous mats) based on biodegradables and ECPs for biomedical applications. On the other hand, it should be remarked that the electrochemical detection of biomolecules using ECPs has received intense interest within the biomedical field.[121–126] In this application, ECPs act as interfaces between bio-substrates and inorganic electrodes favouring lowered impedance between the electrode and electrolyte interface. Accordingly, ECP-based biosensors consist of organic films (or even hydrogels) supported on inorganic electrodes rather than in self-supported organic membranes and, therefore, their discussion has not been included in this review.

Nevertheless, one of the major drawbacks in obtaining free-standing nanosheets composed exclusively of ECPs is the lack of mechanical integrity, poor stability, brittleness and the restricted processability of many of these materials. These limitations, combined with their non-degradability, affect the number of biomedical applications of all-ECP FsNMs. Because of this reason, in this section we separate the few studies on FsNMs fabricated only with ECPs and inorganic–ECP hybrids, from those based on insulating polymer–ECP blends.

The biomedical applications of some ECPs are limited by the biocompatibility and cytotoxicity of these materials, which in turn depend on their chemical nature. In a recent study, Humpolicek *et al.*[127] examined the biocompatibility of non-conducting and conducting PAni forms (*i.e.* PAni emeraldine base and PAni hydrochloride, respectively). Although both forms of PAni did not induce any sensitization and skin irritation, the two materials but especially PAni hydrochloride exhibited considerable cytotoxicity. Polymer purification *via* re-protonation ↔ de-protonation cycles led to a significant reduction in cytotoxicity, suggesting that the negative effects were provoked by low molecular weight reaction residues or by oligomers rather than by the own PAni molecules. Subcutaneous implantation of PAni emeraldine base films into animal models showed inflammation response and fibrous encapsulation.[128,129] In opposition, PPy exhibited good biocompatibility. Wang *et al.*[130] evaluated the biocompatibility of PPy supported membranes with nerve tissue. PPy showed no evidence of acute and subacute toxicity, pyretogen, hemolysis, allergen and mutagenesis, and the cells showed better survival and proliferation rates than with the control saline solution. These results suggested that PPy might be a candidate material for bridging the peripheral nerve gap.[130]

George *et al.*[131] evaluated the cytotoxicity of PPy *in vitro* using primary cerebral cortical cells and *in vivo* surgically implanting PPy substrates in the cerebral cortex of rats. The results evidenced that PPy is at least as biocompatible as Teflon (used as a control) and, in fact, performed better in many cases. Similarly, PTh and its derivatives have shown tremendous potential for interfacing electrically conducting polymers with biological applications due to their low cytotoxicity and high biocompatibility. For example, PEDOT[41] and poly(α-terthiophene)[132] (PTh_3) have been used to fabricate bioactive platforms, even though their monomers and small oligomers are cytotoxic. Cytotoxicity is particularly low for some water-soluble PTh derivatives bearing hydrophilic pendant moieties, which have been proposed as excellent lysosome-specific materials for bio-imaging applications.[133]

Despite its current importance among conducting materials and its recently developed biomedical applications, in this review we have not included studies based on graphene nanosheets.[134,135] Graphene typically presents porous and honeycomb-like structures and, in some cases, it has been considered as an alternative to ECPs in the preparation of single component FsNMs. However, the use of graphene is restricted by the topology of its bidimensional nanosheets, which is not comparable to that of ECPs.[136,137]

5.1. All-electroactive conducting polymers and inorganic-electroactive conducting polymer free-standing nanomembranes

In spite of the fact that the mechanical properties of ECPs are in general poor, different strategies have been developed to produce free-standing membranes of micrometric thickness made of PPy,[138–142] PAni[143–145] and PTh[146–148] for their application in different fields, such as separation membranes, electrode materials, sensors and catalysts.

 This journal is © The Royal Society of Chemistry 2015

Open Access Article. Published on 28 May 2015. Downloaded on 4/2/2026 11:03:23 AM.
This article is licensed under a Creative Commons Attribution 3.0 Unported Licence.

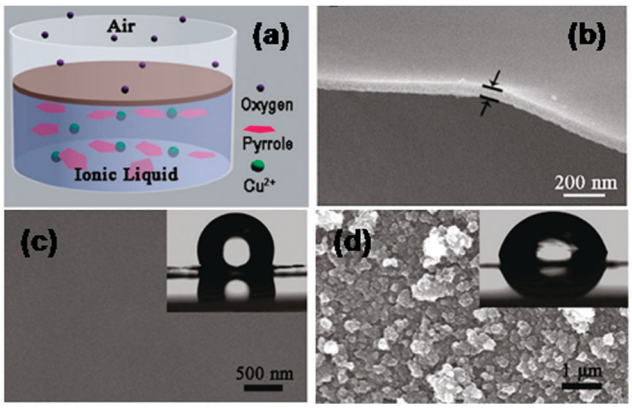

Fig. 13 (a) Schematic illustration of the formation of a film at the air/ionic liquid interface. (b) High magnification of the cross-sectional SEM images of the PPy FsNM. Top-view SEM image of (c) the rough side and (d) the smooth side of the film. (inset) Water contact angle, showing values of 115° and 80° for the rough and smooth sides, respectively. Reproduced with permission.[149] Copyright 2010, American Chemical Society.

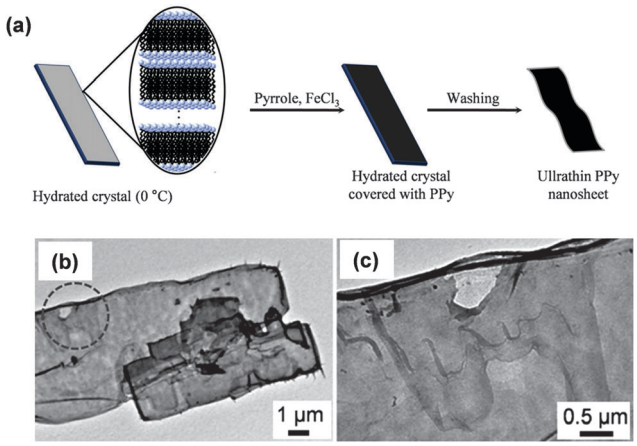

Fig. 14 (a) Schematic illustration of the synthesis procedure for PPy FsNMs using hydrated crystals of sodium decylsulfonate. (b) TEM image of PPy FsNMs. (c) Magnified image of the circle displayed in (b). Reproduced with permission.[150] Copyright 2011, Elsevier.

In 2010, Wang *et al.*[149] reported a novel one-pot procedure to prepare PPy FsNMs which was based on an interfacial polymerization (IP) that occurred at the interface between air and a Cu^{2+}-containing ionic liquid (Fig. 13a). Resulting films were compact and uniform, and exhibited finely controlled thickness, with values from tens to hundreds of nanometers (*i.e.* as low as 60 nm, Fig. 13b). However, FsNMs with a thickness under 50 nm were brittle and weak, and broke easily. PPy FsNMs doped with *p*-toluenesulfonic acid (TSA) displayed good electrical properties. Specifically, the electrical conductivity of films with a thickness of ~230 nm was 1.14 S cm^{-1}, although this value was lower than that reported previously for PPy in other systems. Moreover, asymmetrical films with different smoothness and water wettability on each side of the film were also prepared by altering the concentration of Cu^{2+} ions in the liquid phase (Fig. 13c). Even though no biomedical application was proposed by the authors, it is highly promising for this field the development of a general methodology for the preparation of ECP films with different hydrophilicity and roughness on each side.

Jeon *et al.*[150] fabricated PPy FsNMs by organic crystal surface-induced polymerization of the monomer in an aqueous suspension containing hydrated crystals of sodium decylsulfonate below the Krafft temperature (*i.e.* temperature above which thermodynamic stable micelles are formed), and using $FeCl_3$ as the oxidant (Fig. 14a). The main role of the crystals was to act as a template onto which the polymerization occurred. FsNMs obtained using this procedure were composed of a unique ECP domain with a thickness of ~21 nm, widths of 2–6 μm, and lengths greater than 10 μm (Fig. 14b and c). The electrical conductivity of these nanosheets was determined to be 30.6 S cm^{-1}, thus one order of magnitude higher than the value displayed by spherical PPy nanoparticles (diameters 30–50 nm) prepared by emulsion polymerization (2.9 S cm^{-1}). Besides, the feasibility of PPy FsNMs to perform as HCl and NH_3 vapour detectors was evaluated: the system exhibited high sensitivity and a fast response with respect to PPy nanoparticles, which was attributed to the increased surface area and porosity of the former nanostructure. Despite the fact that the application studied for PPy FsNMs was not biologically related, the methodology used is of relevant importance to successfully obtain FsNMs.

More recently, Qi *et al.*[151] developed PPy FsNMs by *in situ* freezing interfacial polymerization (FIP). This approach differs from the conventional interfacial polymerization in that the chemical reaction takes place at a solid/liquid interface. In this specific work, water and cyclohexane, which are immiscible, were used as the liquid and solid phase, respectively, solid cyclohexane being achieved upon crystallization. Special attention was paid to the following issues: (1) the reaction temperature, which should be lower than the freezing point of the organic solvent and water, but above that of the monomer; and (2) the minimization of the polymerization of the monomer and the formation of PPy particles before the formation of solvent crystals. FsNMs were very smooth and their thickness was about 100 nm. In this case, the electrical conductivity was determined to be 430 S cm^{-1}, whereas for the optimal synthetic conditions and doping parameters, the electrical conductivity reached peaks as high as 2010 S cm^{-1}, opening the door to potential biomedical applications such as biosensors.

Jha *et al.*[152] reported a novel strategy for the one-pot fabrication of PPy FsNMs by adding dropwise a dichloromethane solution that contained the monomer and a porphyrin derivative to an aqueous $FeCl_3$ solution kept in a beaker. Initially, a porphyrin–PPy bilayer formed spontaneously at the air/$FeCl_3$ interface, which after being washed rendered the PPy nanosheet. Following this method the nanosheet thickness can be tailored by changing the monomer concentration in the dropping solution. Hence, the thickness of the PPy FsNM prepared by Jha *et al.*[152] increased from 50 to 250 nm when the pyrrole concentration augmented from 0.01 to 1 M. In addition, the conductivity of these PPy FsNMs, which was initially only

Open Access Article. Published on 28 May 2015. Downloaded on 4/2/2026 11:03:23 AM.
This article is licensed under a Creative Commons Attribution 3.0 Unported Licence.

$\sim 10^{-5}$ S cm^{-1}, was enhanced after optimizing the doping parameters (*i.e.* the conductivity improved by $\sim$30 and $\sim$150 times on exposure to hydrochloric acid and iodine, respectively). Most importantly, the conductivity of these nanosheets showed no change when kept in air for more than 6 months, revealing a very noticeable stability in air. Although no specific application was examined, potential applications were mentioned (*e.g.* biosensors and artificial muscles).

On the other hand, the number of studies devoted to PAni-based nanosheets, which mainly consist of PAni–inorganic hybrid composites, is very scarce and their application in the biomedical field is practically inexistent. For example, very recently, the fabrication of layered PAni–graphene–PAni nanosheets (the thickness of PAni and graphene layers was 3.7 and 8.9 nm, respectively), which exhibited excellent gravimetric capacitance, was reported.[153] This sandwiched structure was essentially oriented towards applications in energy storage devices, solar cells, semiconducting devices, *etc.* Niu *et al.*[154] used a "*skeleton/skin*" strategy for the preparation of free-standing, thin and flexible single-walled carbon nanotube (SWCNT)–PAni hybrid films by a simple *in situ* electrochemical polymerization method. In this approach, directly grown SWCNT films with a continuous reticulate structure acted as the template, whereas PAni layers acted as the skin. The resulting hybrid films displayed a much higher conductivity compared to that of SWCNT–PAni composite films based on the post-deposition of the SWCNT film. Flexible, thin and lightweight supercapacitors were fabricated using SWCNT–PAni hybrid films. Although the applications of PAni-based nanomembranes[153,154] were not related with biomedicine, the above described properties may be useful for the fabrication of energy storage components for biomedical equipment.

Regarding PTh and its derivatives, Greco *et al.*[155] reported the preparation of FsNMs made of PEDOT and PSS complexes (PEDOT–PSS), where PSS acted as the doping agent. In this study, the supporting layer method, which enables the release and recovering of the free-standing nanosheet, was used (Fig. 15). Firstly, a layer of water-soluble PVA is deposited as the sacrificial layer on a substrate (PDMS) by spin-coating. Then, the desired nanosheet is supported on that sacrificial layer. Later, once the bilayered film is dried, it is peeled off from the substrate. The thickness of those FsNMs, which was controlled through the rotation speed, ranged from $\sim$100 nm (rotation speed of 1000 rpm) to $\sim$40 nm (rotation speed $\geq$ 4000 rpm). Moreover, the mechanical and electrical properties of PEDOT–PSS FsNMs were extensively investigated as a function of their thickness. With decreasing thickness, the elastic modulus values, which were determined by the strain-induced buckling test, varied between 0.81 and 1.02 GPa, while the electrical conductivity decreased from 1.44 to 0.88 S cm^{-1}. Interestingly, solvent cast PEDOT–PSS micrometric films (a thickness of 7.5 μm) showed a conductivity of 1.38 S cm^{-1}. Therefore, a percolation threshold was reached based on the microscopic grain-like structure or the effect of residual water present in the FsNM. This is schematically illustrated in Fig. 16, which shows that the interconnectivity between neighbour

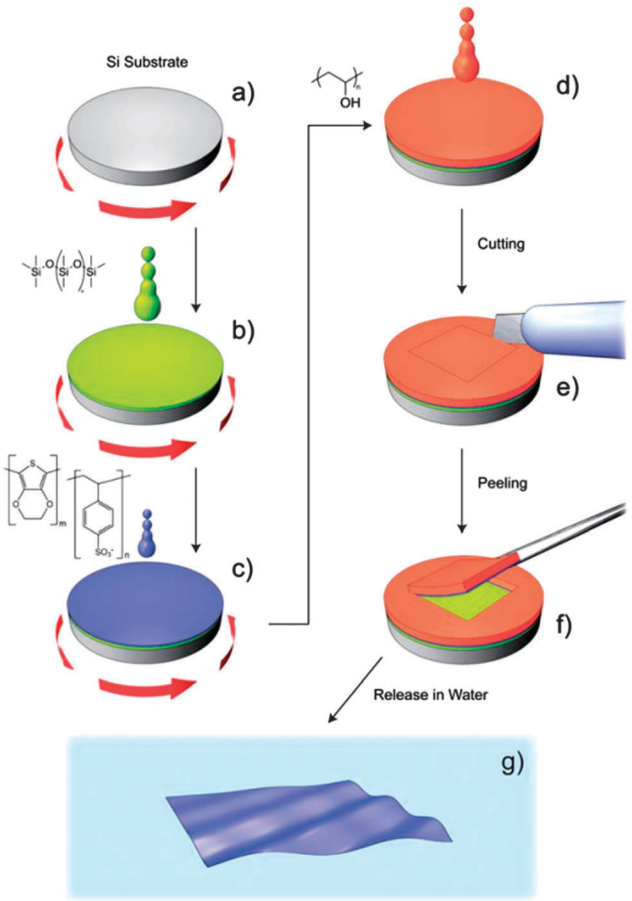

Fig. 15 Schematic representation of the main steps of fabrication and release for obtaining PEDOT–PSS nanofilms by a supporting layer technique. (a) Si substrate; (b) spin-coating deposition of the PDMS substrate layer; (c) spin-coating deposition of the PEDOT–PSS nanofilm; (d) casting of a thick PVA supporting layer; (e) cutting and (f) peeling of the bilayer (PVA supporting layer + PEDOT–PSS nanofilm); (g) freestanding PEDOT–PSS nanofilm floating in water after dissolving PVA. Reproduced with permission.[155] Copyright 2011, The Royal Society of Chemistry.

conductive particles is not improved in FsNMs with increasing thickness. However, the stacking of multiple conductive grains in micrometric films results in an improved number of interconnections and long-range connectivity. Because of the proven biocompatibility of PEDOT,[41,156,157] PEDOT–PSS FsNMs were considered as first proof of concept towards the development of smart conductive substrates for cell growth and stimulation.[155] Although no cell culture study was reported in that work, PEDOT–PSS FsNMs have been recently used to fabricate electrochemical microactuators in the form of microfingers with a variety of lengths.[158] The reversible actuation of these microactuators, which consists in the bending of such microfingers, has been demonstrated by imposing electrochemical oxidation and reduction cycles on PEDOT–PSS supports. A number of possible applications can be envisaged for these small, soft actuators, such as microrobotics for cell manipulation.

The same group embedded iron oxide superparamagnetic nanoparticles into PEDOT–PSS FsNMs using the supporting layer method described above (Fig. 15).[159] More specifically, a

 This journal is © The Royal Society of Chemistry 2015

Open Access Article. Published on 28 May 2015. Downloaded on 4/2/2026 11:03:23 AM.
This article is licensed under a Creative Commons Attribution 3.0 Unported Licence.

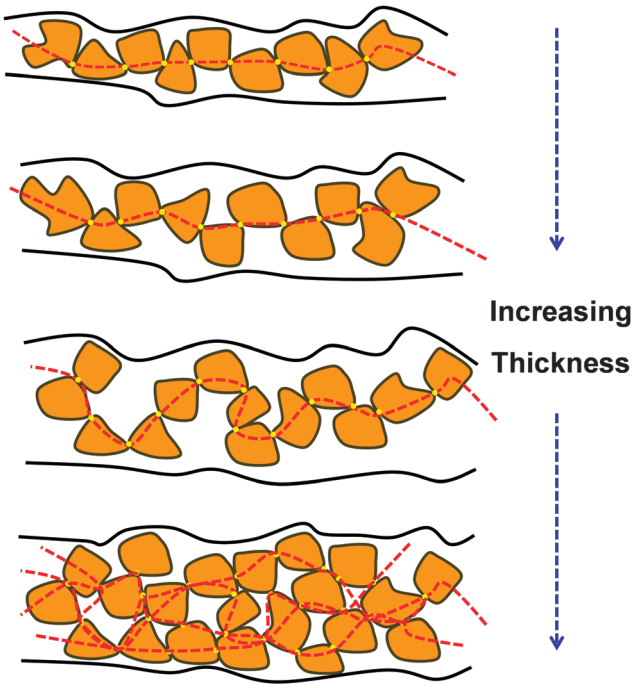

Fig. 16 Schematic representation of the nanofilm structure made up of PEDOT-rich particles (orange) surrounded by the PSS matrix. The suggested percolative mechanism in nanofilms as thickness increases is depicted; the length of conductive pathways between neighbor PEDOT particles (dashed red line) increases with thickness up to a percolation threshold, when multiple parallel pathways become available.

stable colloidal dispersion of iron oxide nanoparticles added to the PEDOT : PSS mixture was used to prepare nanofilms through spin-coating. The thickness and surface roughness of the nanosheets depended on the amount of incorporated nanoparticles, ranging from 218 ± 13 to 269 ± 19 nm and from 1.5 to 8.5 nm, respectively. In this investigation, the attention was focused on the characterization of the morphological, electrical, magnetic and magneto-optical properties, which also depended on the amount of entrapped iron oxide nanoparticles. The electrical conductivity was found to decrease from 1.96 ± 0.14 S cm^{-1} to 0.38 ± 0.06 S cm^{-1} with increasing concentration of nanoparticles. These FsNMs open up new perspectives in technological fields (electronics, telecommunications and optics) than can be successfully used for the construction of biomedical devices, even though no practical evidence for any application was provided.

PEDOT–PSS was also employed by Greco *et al.*[160] to prepare and characterize robust wrinkled conductive surfaces. This was achieved by following the simple two-step approach (metal deposition and subsequent heating) developed for the fabrication of nanowrinkles on shape-memory polymer sheets.[161] Specifically, the ECP nanosheet (thickness ranging from 53.6 ± 1.2 to 120.9 ± 1.5 nm) was deposited onto a thermo-retractable PS sheet by spin-coating an aqueous dispersion of PEDOT:PSS. A subsequent thermal treatment induced the substrate shrinking causing the microbuckling of the upper PEDOT:PSS layer due to compressive stress patterning. Adhesion and proliferation assays of C2C12 murine skeletal cells on uniaxial wrinkled samples indicated that cells preferentially aligned on low and narrow ridges (~1.5 μm in height) rather than on high and wide ones (~2.5 μm in height). This observation was corroborated when aligned myotubes in the C2C12 differentiation stage were only formed on the former topology. Furthermore, the co-culturing of C2C12 cells with a fibroblast feeder layer improved the formation of aligned and mature myotubes. The achievement of tuneable conductive nanowrinkled interfaces represents a unique tool for the development of innovative biomedical devices.

PEDOT has also been used to prepare mechanically robust, electrically conductive and transparent hybrid FsNMs. This was achieved by Lee *et al.*,[162] who coated densified carbon nanotube sheets with PEDOT by vapour phase polymerization. For FsNMs with a thickness of ~66 nm, the main properties were high mechanical strength and modulus (135 MPa and 12.6 GPa, respectively), low resistance (below 200 Ω per square), moderate

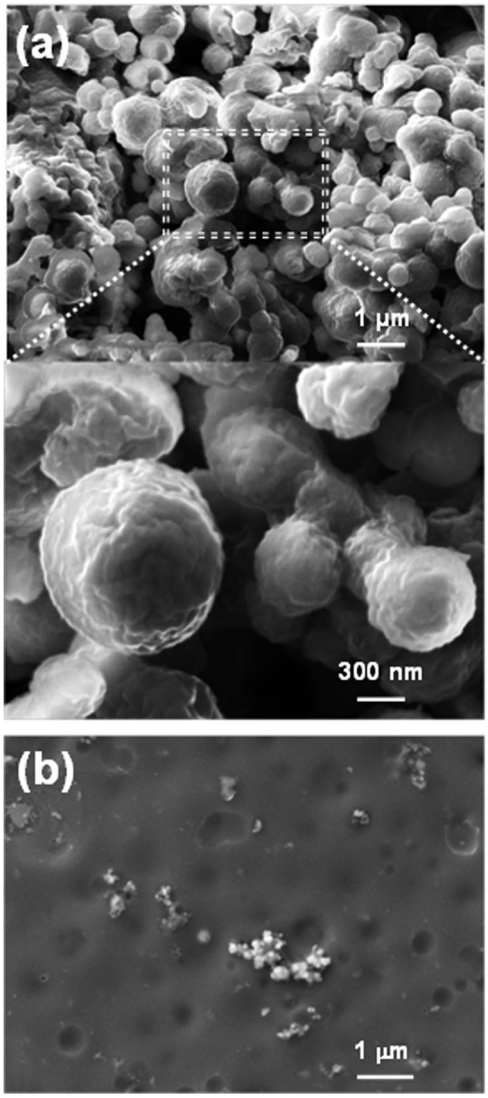

Fig. 17 (a) Low (top) and high (bottom) magnification SEM micrographs of P3TMA powder. (b) SEM micrograph of P3TMA nanosheets.

Open Access Article. Published on 28 May 2015. Downloaded on 4/2/2026 11:03:23 AM.
This article is licensed under a Creative Commons Attribution 3.0 Unported Licence.

Table 3 Summary of the most important characteristics (*i.e.* preparation method, thickness, properties and potential biomedical applications) of FsNMs made of ECPs and electrochemically inactive polymers

Material	Preparation	Thickness (nm)	Properties[a]	Biomedical applications	Ref.
PPy	Interface polymerization	From 60 to hundreds	σ = 1.14 S cm^{-1} for a thickness of 230 nm. Flexible, transparent, shiny and light-blue color.	Those in which films with different roughness and water wettability on each side of film fit	149
PPy	Organic crystal surface-induced polymerization	~21	σ = 30.6 S cm^{-1}. Smooth surface	Chemical sensors, successful results being obtained with HCl and NH_3 vapors	150
PPy	*In situ* FIP	~100	Extremely high electrical conductivity with σ = 2000 S cm^{-1}. Semi-transparency and smooth surface	Fabrication of sensors	151
PPy	Interface polymerization using porphyrin as an *in situ* template	From 50 to 250	Low conductivity ($\sigma \approx 10^{-5}$ S cm^{-1}) that can be adjusted by doping. Mechanically strong and dense morphology	Biosensors and artificial muscles	152
PEDOT–PSS	Supporting layer	From ~40 to ~100	Conductivity, (σ = 0.88–1.44 S cm^{-1}) comparable to that of micrometric films (σ = 1.38 S cm^{-1}). E = 0.81–1.02 GPa. Flexibility.	Bioactive platforms. Electrochemical soft microactuators (microfingers) for cell manipulation with microrobots	155 and 158
PEDOT–PSS	Spin-coating + heat-shrinking process	From 53.6 ± 1.2 to 120.9 ± 1.5	R = 199 ± 11–586 ± 16 Ω per square presence of anisotropic topographical cues at the micro- and nanoscale on the surface	Smart scaffolds for functional cell alignment and electrical stimulation.	160
PEDOT–carbon nanotube sheets	Vapor phase polymerization	~66	R = 200 Ω per square. E = 12.6 GPa, σ_{max} = 135 MPa. Volumetric capacitance: ~40 F cm^{-3} at 100 V s^{-1}. Flexibility and transparency.	Sensors and actuators	162
PE44–P3TMA	Spin-coating	From 20 to 80	$\sigma = 10^{-4}$ to 10^{-5} S cm^{-1} depending on the composition of the blend. Robustness, flexibility and transparency. Yellowish color. Biodegradable and electro-compatible with cells.	Bioactive platforms with semiconducting response for tissue regeneration.	167 and 168
TPU–P3TMA	Spin-coating	From 11 to 93	σ = from 2.23 × 10^{-5} to 5.19 × 10^{-6} S cm^{-1}, current = from 0.43 to 1.85 pA. E = 0.9–1.7 GPa, $F_{adh} \approx 6$ nN. ε_g = 2.35 eV. Robustness, flexibility and transparency. Yellowish color. Biodegradable and electro-compatible with cells.	Bioactive substrates for advanced biomedical applications	169–171
(PEDOT–PSS)–PLA	Spin-coating	~45 (PEDOT–PSS layer) + ~200 (PLA layer)	σ = 180 S cm^{-1}. Mechanical robustness and conformability. Colors from dark blue to light blue or even transparent depending on the oxidation state. Electrochemical regulation of the surface wettability.	Smart conductive biointerfaces for directing cell adhesion and differentiation. Bioelectrodes.	172
(TPU–P3TMA)–collagen	Spin-coating + adsorption	From 11 to 93 (TPU–P3TMA layer) + 73 (collagen layer)	Formation of a pseudoregular honeycomb 2D network, in which the top layer resembled a fibril structure	Three-dimensional scaffolds for tissue engineering	171

[a] σ: electrical conductivity. R: electrical resistance. E: elastic modulus. σ_{max}: ultimate tensile strength. F_{adh}: adhesion force between the AFM tip and the sample surface. ε_g: optical band gap energy.

This journal is © The Royal Society of Chemistry 2015

Open Access Article. Published on 28 May 2015. Downloaded on 4/2/2026 11:03:23 AM.
This article is licensed under a Creative Commons Attribution 3.0 Unported Licence.

optical transparency (56% at 550 nm wavelength), high flexibility and minor changes in resistance upon bending. Another interesting characteristic of these FsNMs was their remarkable shape-recovery ability in a liquid and at the liquid/air interface, as opposed to previous carbon nanotube sheets. On the basis of these properties, these hybrid PEDOT-containing FsNMs were proposed to be of potential interest in the design of sensors, actuators, optical devices, and fuel cells, as well as for electrochemical capacitors.

Ultra-thin films (a thickness of 47 nm) of poly(3-thiophene methyl acetate) (P3TMA) have been prepared by spin-coating. For this system, the remarkable influence of the film–air interface on the thermal properties was examined by comparing the response of nanosheets and bulk P3TMA powder.[163] Although P3TMA, which is soluble in tetrahydrofuran, chloroform and dimethylformamide, among a few others, does not form free-standing films,[164] the understanding of its properties is of great interest because, as it will be discussed in the next sub-section, P3TMA has been combined with conventional biodegradable polymers to fabricate different types of electroactive FsNMs with biomedical applications. Interestingly, the glass transition temperature determined using microcantilevers coated with ultra-thin P3TMA films resulted in 5.2 °C higher than that obtained for bulk powder samples. Moreover, ultra-thin films showed nanospherical aggregates of small (~40 nm) size, while powder bulk samples presented a micrometric granular morphology (Fig. 17).

5.2. Insulating polymer-electroactive conducting polymer free-standing nanomembranes

As mentioned above, blending of ECPs with insulating polymers is the most commonly followed approach to overcome the poor mechanical integrity of organic semiconductors. Accordingly, free-standing membranes have been fabricated by solvent casting mixtures of ECPs with conventional insulating polymers, such as PVA[144] and nylon 66.[165] However, in all cases, such membranes were of micrometric thickness and their potential use (*e.g.* optical pH sensors[144] and conductive coatings[165]) was not related to the biomedical field, even though they were prepared by combining ECPs with biopolymers derived from natural sources. For example, cellulose–PAni membranes of micrometric thickness, which were prepared by *in situ* polymerization of aniline in the presence of bacterial cellulose nanofibrils, were used as electromagnetic interference shielding materials despite the biological origin of the biopolymer.[166] Table 3 summarizes the most relevant examples of ECP-containing FsNMs, discussed in this section.

Armelin *et al.*[167] reported the preparation and characterization of FsNMs that were obtained by spin-coating mixtures of a biodegradable polyester, poly(tetramethylene succinate) (PE44), and P3TMA. The thickness of these ultra-thin membranes, which ranged from 20 to 80 nm, was precisely controlled by adjusting the spin-coating process parameters and the solution concentration. It was proved that PE44–P3TMA FsNMs retained both the biodegradability of PE44 and the semiconducting ($\sim 10^{-4}$ S cm^{-1}) and electrochemical properties of P3TMA. Calorimetric assays revealed that P3TMA and PE44 were only partially miscible, evidencing a phase separation. Thus, two glass transitions were identified in the mixture, even though they depended on the composition of PE44–P3TMA FsNMs. Furthermore, the presence of P3TMA hindered the crystallization of PE44 and also affected the fusion of the PE44 crystalline fraction. Nanosheets were found to be stable in air and ethanol for more than one year, which facilitates their manipulation. Preliminary cell culture results using epithelial cells (HEp-2) suggested that PE44–P3TMA FsNMs are potential candidates for the fabrication of bioactive platforms with semiconducting response.

The good results obtained for PE44–P3TMA FsNMs prepared using a 50 : 50 PE44 : P3TMA molar ratio motivated further study on their potential application in the biomedical field. More specifically, Pérez-Madrigal *et al.*[168] conducted an investigation devoted to quantifying the following aspects related to these nanosheets: (1) their hydrolytic and enzymatic degradability; (2) their response towards different fibroblast and epithelial cellular lines; and (3) their electrochemical response when coated with cell monolayers. Hydrolytic and enzymatic degradation assays revealed the appearance of abundant crevasses and thin grooves after 4 weeks of immersion in phosphate buffered saline solution (PBS), and these effects become more pronounced after 8 weeks (Fig. 18a). Moreover, the weight loss of samples immersed in hydrolytic and enzymatic media indicates that the degradation rate is higher for the PE44–P3TMA blend than that for the individual polyester (Fig. 18b). This was attributed to the fact that in the blend the degradation of the polyester domains produced the detachment of P3TMA domains (labelled with white circles in Fig. 18a). On the other hand, *in vitro* cellular adhesion and proliferation assays using HEp-2, MDCK, Cos-7 and Du-145 cell lines evidenced that PE44–P3TMA nanosheets behaved as potent cellular matrices (Fig. 18c). Thus, the viability of cultured cells was higher, in terms of adhesion and proliferation, in blended FsNMs than in individual PE44 and P3TMA ultra-thin films. Moreover, cyclic voltammetry studies reflected that PE44–P3TMA FsNMs were electrocompatible with cellular monolayers, even though there was a slight reduction in the cathodic and anodic intensities. These features combined with the outstanding flexibility and robustness of the nanomembranes, which was demonstrated through aspiration in pipette/release/shape recovery cycles that were repeated without breaking the film (Fig. 19), allowed the authors to propose the use of biodegradable PE44–P3TMA FsNMs as bioactive platforms for tissue engineering.

Inspired by those promising results, Pérez-Madrigal *et al.*[169] replaced the polyester component in the preparation of PE44–P3TMA FsNMs by an aromatic grade thermoplastic polyurethane matrix (TPU). This was expected to improve the miscibility between the two components of the blend because of the presence of aromatic moieties in both polymers. Hence, TPU–P3TMA FsNMs were prepared by spin-coating a TPU : P3TMA mixture with a 40 : 60 weight ratio. The surface of the resulting nanosheets was described to be the combination of the topographies of both individual components. This consisted of a

Open Access Article. Published on 28 May 2015. Downloaded on 4/2/2026 11:03:23 AM.
This article is licensed under a Creative Commons Attribution 3.0 Unported Licence.

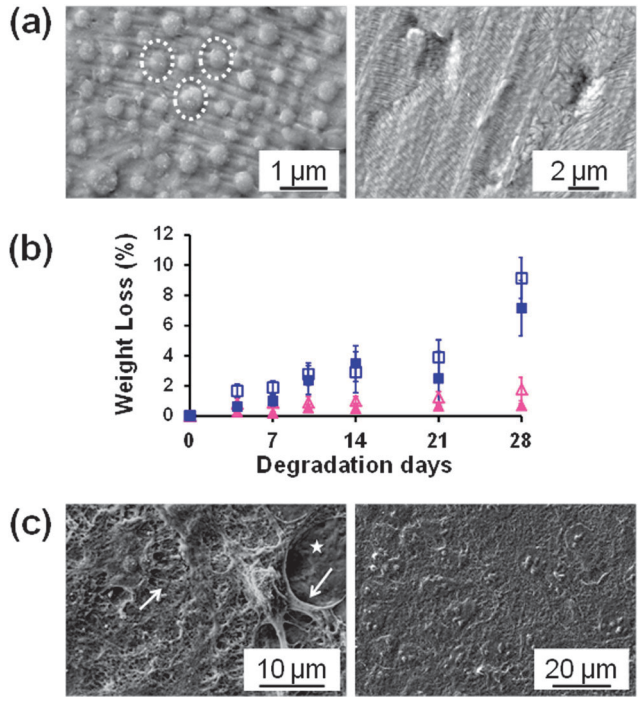

Fig. 18 (a) SEM micrographs of hydrolytically degraded PE44–P3TMA FsNMs (blend prepared using a 50 : 50 molar ratio) after 4 weeks (left) and 8 weeks (right) of immersion in PBS. Circles show the conductive phase (spherical aggregates of P3TMA). (b) Plot of the weight loss (%) *versus* the degradation time (days) in hydrolytic (filled symbols) and enzymatic media (empty symbols) for PE44 (triangles) and PE44–P3TMA (squares) films. (c) SEM micrographs of Cos-7 (left) and Du-145 (right) cells adhered on the surface of PE44–P3TMA nanomembranes. The film surface (domains without cells) is shown by asterisks (*), while the connections or interactions between the cell and the surface or between two cells are indicated by arrows.

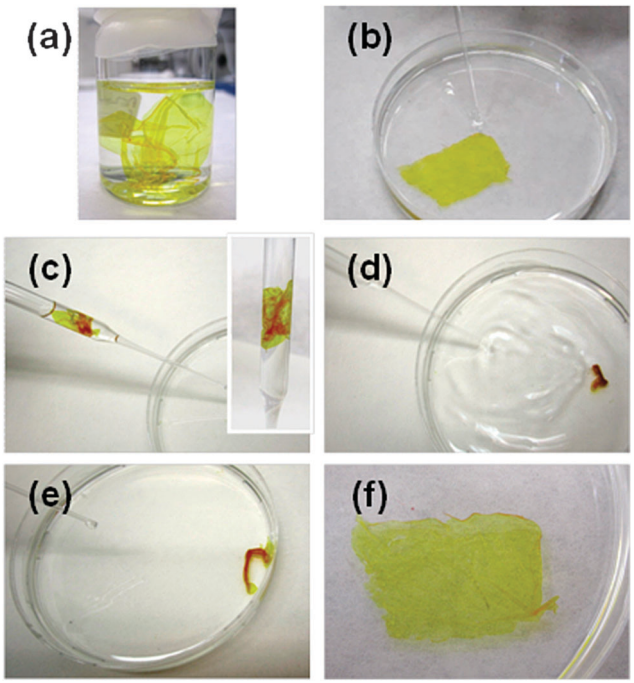

Fig. 19 (a) Digital camera image of a PE44–P3TMA FsNM immersed in ethanol; (b–c) aspiration of the nanomembrane floating in ethanol into a pipette; (d–e) release of the folded nanomembrane into the ethanol solution; and (f) aspect of the nanomembrane after recovering the shape.

homogeneous distribution of granules throughout the surface, which were associated with the P3TMA rich phase by conductive AFM (C-AFM) measurements (Fig. 20). Moreover, TPU–P3TMA nanosheets showed homogeneously distributed well-localized folds, similar to those also observed in individual TPU FsNMs. As some films did not present folds, their formation was attributed to artefacts produced during the spin-coating process. The thickness of FsNM TPU–P3TMA ranged from 11 to 93 nm, while the average roughness was 16.3 ± 0.8 nm. Analysis of the mechanical properties indicated that the Young's modulus, which was determined by applying the Derjanguin–Müller–Toporov (DMT) contact mechanics, depended on the thickness of the nanomembranes. Thus, values determined for the thicker (80–140 nm)/thinner (10–40 nm) regions of TPU, P3TMA and blended ultra-thin films were 25/35 MPa, 3.5/12 GPa and 0.9/1.7 GPa, respectively. In contrast, the adhesion force was found to be homogeneous throughout the whole surface of TPU and P3TMA films (average values: 7.2 and 5.0 nN, respectively), while it depended on the phase distribution in the case of TPU–P3TMA FsNMs. The potential utility of these FsNMs for tissue engineering applications was proved by cellular proliferation assays using Cos-7 cells. The results showed that the TPU–P3TMA FsNM was more active as a cellular matrix than each of the two individual polymers.

In a subsequent study, the same authors[170] examined the electronic, electric and electrochemical response of the above mentioned TPU–P3TMA FsNM. Interestingly, the optical band gap energy of these blended nanofilms was very similar to that obtained for individual P3TMA (*i.e.* E_g = 2.35 and 2.32 eV, respectively). This similarity, which did not occur when comparing the E_g value of the TPU : P3TMA mixture with that of P3TMA dissolved in THF, was attributed to the influence of the spin-coating process on the π-conjugation length and packing interactions of P3TMA chains (*i.e.* ECP chains are not able to adopt their equilibrium conformation because the solvent is completely evaporated). On the other hand, the electrical conductivity of TPU–P3TMA FsNMs, determined by C-AFM measurements, was found to range from 2.23×10^{-5} to 5.19×10^{-6} S cm^{-1}. These inhomogeneous values were consistent with the presence of insulating TPU chains in P3TMA-rich domains. The voltammetric response of TPU–P3TMA FsNMs and P3TMA was similar in terms of the ability to exchange charge reversibly and their electrochemical stability. On the basis of these results, the authors proposed that TPU–P3TMA FsNMs were excellent candidates to be used in tissue regeneration applications as biointerfaces to conduct electrical or electrochemical stimulation.[170]

Following this research line, in a very recent study,[171] special emphasis was given to determine the influence of the TPU–P3TMA FsNM composition on those properties typically related

 This journal is © The Royal Society of Chemistry 2015

Open Access Article. Published on 28 May 2015. Downloaded on 4/2/2026 11:03:23 AM.
This article is licensed under a Creative Commons Attribution 3.0 Unported Licence.

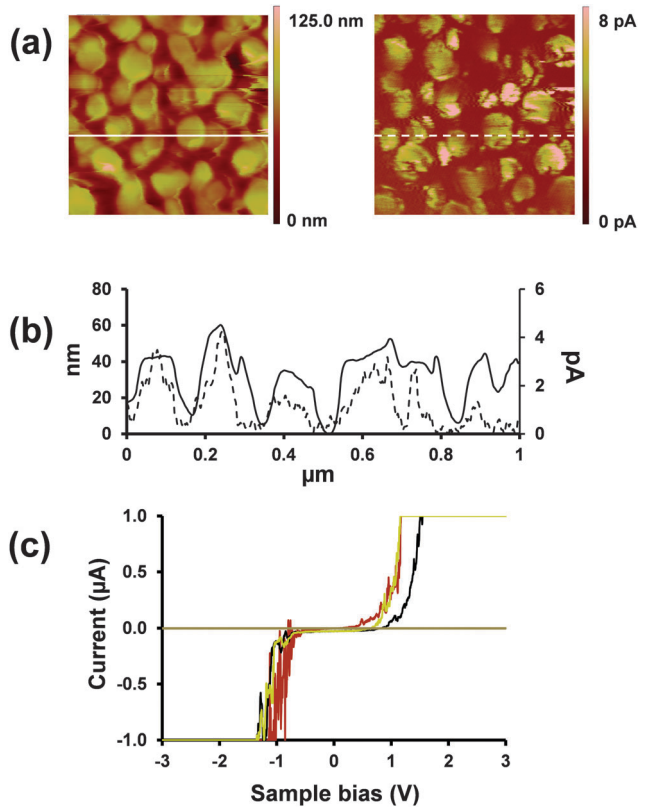

Fig. 20 C-AFM characterization for TPU–P3TMA (40 : 60) nanomembranes deposited onto ITO: (a) simultaneous 1 μm × 1 μm topographical image (left) and C-AFM current image (right) for the same sample. (b) Dual cross-section profile of the above images indicating variations in height (solid line) and current (dashed line). (c) Typical current–voltage curves (100 nA/div amplifier, max top current 1 μA).

to biomedical applications, such as swelling, resistance to hydrolytic and enzymatic degradation, and biocompatibility. Therefore, TPU–P3TMA FsNM samples with different TPU : P3TMA compositions (20 : 80, 40 : 60 and 60 : 40 weight ratios) were studied. Structural investigations based on morphological and topographical analyses evidenced that the 20 : 80 sample exhibited a surface similar to that obtained for individual P3TMA, while 40 : 60 and 60 : 40 FsNMs presented an irregular distribution of prominent and well-localized folds like individual TPU. The water uptake of nanosheets decreased with the concentration of TPU, even though it was relatively high in all cases. Consistently, hydrolytic and enzymatic degradation increased with the P3TMA content (Fig. 21a and b). Moreover, TPU–P3TMA blends behaved as biodegradable materials. Viability assays evidenced that, although all TPU–P3TMA compositions provided biocompatible blends, the viability of cells increased with the concentration of TPU in the composition (Fig. 21c and d). The overall results allowed the authors to conclude that the 40 : 60 TPU–P3TMA FsNM was the most appropriate system for tissue engineering applications.

A completely different strategy to obtain FsNMs made of an ECP and an insulating polymer is the one in which both components are arranged in a bilayered configuration. Greco *et al.*[172] fabricated self-supported nanosheets with patterned conductivity using PEDOT–PSS and PLA, which acted as the mechanical support layer, thus maintaining continuity and robustness. In a first step, the PEDOT–PSS layer (a thickness of ~45 nm) was spin-coated onto a substrate. Then, in a second step, and after thermal treatment, the PLA layer (a thickness of ~200 nm) was spin-coated onto the previous one. Nevertheless, *n* order to obtain a patterned bilayer FsNM, an intermediate step (inject patterning) was introduced just before the deposition of the PLA layer (*i.e.* localized over-oxidation of PEDOT–PSS nanofilm to provoke an irreversible loss of electrical conductivity at specific spots). Moreover, to enhance its electrical conductivity, which reached a value of 180 S cm^{-1}, DMSO was added as a secondary doping agent. The resulting bilayered FsNM is of great interest as a (bio)electrical interface and as a thin floating or ultraconformable circuit. In addition to that, the surface wettability of the bilayered FsNM was electrochemically switched through simple oxidation and reduction processes. This change was even more evident for nanosheets supported on a PS substrate. On the basis of this interesting ability, the authors proposed the application of these FsNMs as smart conductive biointerfaces for directing cell adhesion and differentiation.[172]

A similar approach was followed by Pérez-Madrigal *et al.*[171] to prepare bilayered FsNMs made of TPU–P3TMA and collagen. However, in this case, the role of the collagen layer was not to provide robustness, which was an intrinsic property of TPU–P3TMA FsNMs, but to enhance the cellular response towards the TPU–P3TMA biointerface. Therefore, the TPU–P3TMA/collagen bilayer was formed by incubating a spin-coated TPU–P3TMA (40 : 60 weight ratio) layer in a collagen solution. Amazingly, the adsorbed collaged layer was found to form two layers (Fig. 22). The top layer exhibited a pseudoregular honeycomb 2D network with cavities of different diameters (*i.e.* ranging from 194 ± 55 nm to 1.2 ± 0.7 μm) and depths *ca.* 73 nm, whereas, in contrast, collagen adopted a much more compact structure in the bottom layer. According to previous studies,[173,174] TPU–P3TMA/collagen biointerfaces were proposed as suitable scaffolds for biological and biomedical purposes. Similarly, a collagen layer was recently used to inhibit the cytotoxic effects of the remaining monomer leaking from a supported PTh_3 film, the resulting PTh_3/collagen biointerface behaving as bioactive platforms.[132]

5.3. A challenge: electroactive conducting polymer free-standing nanomembranes for energy-based biomedical applications

In the 21st century, fuel cells have emerged as smart storage systems or alternative energy conversion devices due to both their efficiency and lack of pollutant emission in comparison with coal combustion engines.[175] Currently, the development of new materials and fabrication processes to improve the effectivity of fuel cells and reduce their cost is an important area of research within this field. The application of ECPs in fuel cell electrodes was proposed as a promising remedy to solve some of the problems identified in such energy storage

Open Access Article. Published on 28 May 2015. Downloaded on 4/2/2026 11:03:23 AM.
This article is licensed under a Creative Commons Attribution 3.0 Unported Licence.

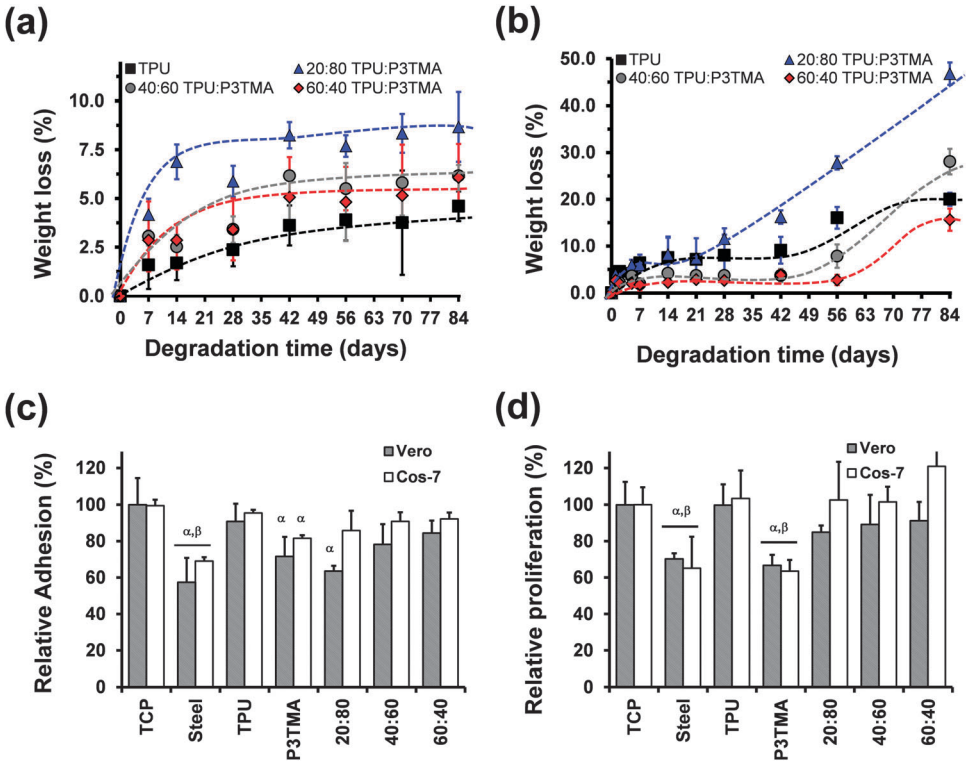

Fig. 21 Weight loss of pure TPU and TPU–P3TMA (20 : 80, 40 : 60, and 60 : 40 ratios) films immersed in (a) PBS solution and (b) lipase-containing PBS solution. Dashed lines were added manually to help following data progression. Relative cellular adhesion (c) and viability (d) on TPU, P3TMA, and TPU–P3TMA (20 : 80, 40 : 60, and 60 : 40 weight ratios) nanomembranes. Assays were carried out using the following cell lines: Vero (shaded bars) and Cos-7 (empty bars). The relative viability was established in relation to the TCP control (tissue culture polystyrene). Steel was also considered as a control substrate because the individual polymers and the blends were deposited on this material. Greek letters on the columns refer to significant differences ($p < 0.05$) using the ANOVA and Tukey test: α *vs.* TCP; β *vs.* steel.

and generation systems, for example chemical long-term stability of the catalytic support and stable mechanical-structural stability.[176] Four different types of applications can be identified depending on the use of ECPs in fuel cell electrodes:

– Support: ECPs as obtained or structured (*e.g.* nanofibers and microspheres) act as a support for the catalyst. For example, Pd–PAni nanofibers showed excellent electrocatalytic activity for the oxidation of methanol, ethanol and formic acid,[177] and Pt incorporated into poly(3-methylthiophene) showed effective dispersion of the catalyst and high catalytic activity in methanol oxidation.[178]

– Coating: the ECP acts as the structured support of another material. For example, graphene nanosheets coated with PAni and decorated with Pt nanoparticles show high activity in the reduction of O_2 and oxidation of methanol, glucose and H_2O_2.[179]

– Part or a composite: for example simultaneous deposition of Pt and Ru on PEDOT doped with polystyrene-4-sulfonate yielded an active electrocatalyst for methanol oxidation.[180,181]

Some of these fuel cell applications of ECPs are based on membranes separating the anodic (fuel) compartment from the cathodic (oxidant) compartment. However, the thickness of polymeric membranes in current fuel cells is on the micrometre scale[176,182] and, therefore, out of the scope of this review. In spite of this, recent advancements in the FsNM field should also be considered as a strong driving force to look for alternative strategies for energy production. The biocompatibility, chemical and dimensional stability, and mechanical properties of FsNMs discussed in previous sub-sections should motivate the scientific community to develop inexpensive and high-performing membranes for the fabrication of biological fuel cells. These devices could be considered from two points of view: (1) macroscopic devices with biological microorganisms participating in the energy production; or (2) biological microorganisms with nanosheets, incorporated as electrode membranes, acting as micrometric biofuel cells. The latter may result in a new field originated by the combination of energy and biomedicine.

Another promising field is the development of artificial muscles using ECP films. In this application, which is based on the transduction of electrical or electrochemical energy into mechanical work, electrochemical reactions in ECP films provoke dimensional variations that result in bending or linear macroscopic movements. The simple way to transduce reversible length variations in films of ECPs into macroscopic movement is through a bilayer ECP/passive layer. The passive layer can be a tape,[183,184] a sputtered metal,[185,186] a piece of paper,[187] ECP/plastic,[188] or a solid state electrolyte.[189] Electrochemically driven length variations in the film of ECP produce stress gradients across the two film interface and subsequently

Open Access Article. Published on 28 May 2015. Downloaded on 4/2/2026 11:03:23 AM.
This article is licensed under a Creative Commons Attribution 3.0 Unported Licence.

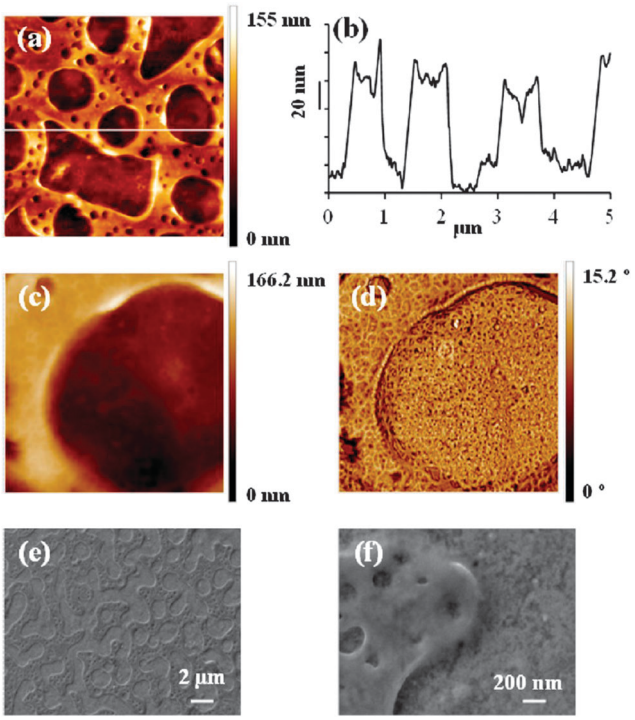

Fig. 22 SEM-AFM images of TPU–P3TMA/collagen nanomembranes: (a) height image 5 × 5 μm^2; (b) cross-sectional data from (a); (c) height image 1 × 1 μm^2; (d) phase image 1 × 1 μm^2 of (c); (e and f) SEM images (14k× and 150k×, respectively). Reproduced with permission.[171] Copyright 2014, American Chemical Society.

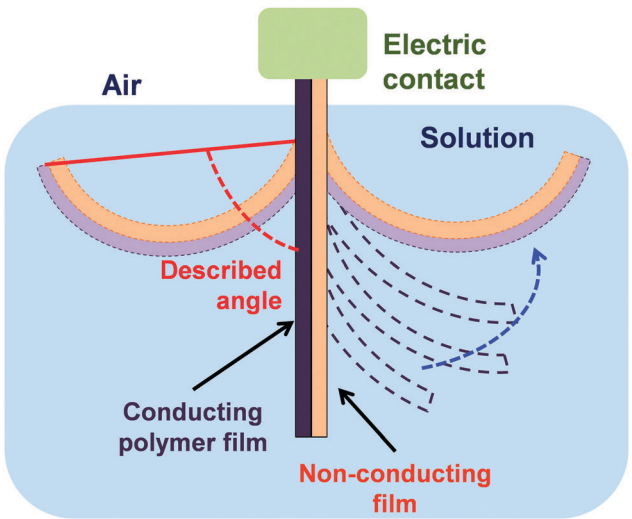

Fig. 23 Scheme of a bilayered artificial muscle device made of ECP adhered on a non-conductive tape. Clockwise and anticlockwise movements are schematically represented by bended dashed lines at left and right, respectively.

result in macroscopic bending, as schematically illustrated in Fig. 23. More specifically, for ECPs exchanging anions with the electrolyte the film gives anticlockwise movement by oxidation (swelling) and clockwise during the reduction, while ECPs exchanging cations produce clockwise movement by oxidation (shrinking) and anticlockwise by reduction of the ECP.[190] Artificial muscles based on ECPs were recently reviewed by Otero and co-workers.[191] Unfortunately, at present time all biomimetic artificial muscles based on ECPs have been prepared using free-standing membranes of micrometric thickness, as occurred for fuel cell electrodes. However, the increasing evolution in biomimetic reactive devices has resulted in the opening of new technological forefronts and challenges, including the application of FsNMs.[191]

6. Conclusions and perspectives

This review of FsNMs for biomedical applications demonstrates the versatility of these simple nanostructures, in which molecules organize in a 2D configuration. Moreover, it highlights several ideas: (i) the variety of techniques available for their preparation, (ii) the concept that the rational design of nanostructured materials can be utilized to obtain tailored properties, and (iii) the relationship between the features of the nanosheets and their applications. Although the list of biomedical applications for self-supported nanosheets is very extensive (*e.g.* wound dressing, patches for bone or tendon repair, scaffolds for regenerative medicine and tissue engineering, magnetically controllable bioactive platforms, drug delivery systems, platelet substitutes, devices for overlapping therapy, artificial soft tissues, biosensors, supports for biological samples, biointerfaces, coatings with microbicide properties, artificial muscles, microactuators for cell manipulation, and bioelectrodes), investigation on such nanostructured organizations is still in its early stages, and many treasures still await scientific discovery.

Research on FsNMs for biomedical applications, which began about one decade ago, has been essentially focused in using insulating polymers. From a practical point of view, studies have been conducted considering only two families of biodegradable materials: (1) polyesters, mainly PLA (*i.e.* PLGA and PE44 nanosheets were also sporadically chosen), and (2) polysaccharides. The inflammatory response provoked by FsNMs made of these materials tends to be very low (*i.e.* lower than that of sutures), which is of particular importance for therapeutic applications. Even though a few studies with other materials have been reported (*e.g.* PEG, PAA, PDDA, P4VPPS and PMMA), these involve polymeric families with very different and disperse properties and, therefore, a general rationalization of the derived conclusions is not an easy task. Within this context, comparative studies to extract general conclusions are imperative. Biomedical applications of FsNMs made of ECPs have emerged with great interest in the last few years (*i.e.* the first work appeared in 2010, even though most studies are from 2013 onwards). Consequently, the number of ECPs studied so far, individually or combined with insulating polymers, is still limited and much more effort is necessary in this direction.

In spite of the studies based on polysaccharides, the preparation of FsNMs by combining synthetic polymers and biomolecules, such as proteins and DNA, is an unexplored

Open Access Article. Published on 28 May 2015. Downloaded on 4/2/2026 11:03:23 AM.
This article is licensed under a Creative Commons Attribution 3.0 Unported Licence.

field. Depending on the desired application, nanosheets with a heterogeneous or homogeneous distribution of the two components (*i.e.* polymer/biomolecule layers or polymer–biomolecule composites, respectively) may be designed. Not only the role played by the polymer in these FsNMs could provide mechanical robustness but also could protect biomolecules against too fast biodegradation. Besides, if it was an ECP, it could also induce electrochemical, electrical or optical activity. However, the biological component would be the main protagonist and, therefore, responsible for the functionality and biomedical applications of such nanosheets. For this purpose, both the number of possibilities and the palette of biocompounds offered by nature are immense. In addition, novel and effective advanced biomedical applications that reach the society cannot be obtained using synthetic polymers alone, thus significant studies related to the combination of synthetic and natural compounds are desirable, and should be a main research focus.

Regarding ECP-containing nanostructured materials, biomedical applications centred on electrophysiology is a field that needs to be further explored. One of the central goals of electrophysiology is to offer tools that can monitor and manipulate bioelectrical activities in the human brain. In particular, implantable neural prostheses aim to replace or restore lost motor functions after disease or disability. Since the brain has soft curvilinear surfaces, properties of conductive FsNMs discussed above are appropriate for the development of flexible bioelectronic interfaces. Hence, by a rational design, flexible ECP-containing FsNMs may be used to establish conformal contact in the cerebral cortex. Another electrophysiological application of these flexible nanosheets is the integration of nanoelectronics in 3D polymer scaffolds for cell cultures. The merging of flexible nanoelectronics and cells would allow the monitoring of biological signals for clinical use.

FsNMs made with unique optical, electrical and magnetic properties can be fabricated using organic–inorganic composites, in which nanoparticles, nanowires, carbon nanotubes, clay platelets or other nanocolloids are combined with insulating or conducting polymers. Although a few studies have been reported in this field, developments are still at a very early stage. For example, organic–inorganic nanosheets could be interfaced with proteins and cells to produce complexes of nanostructured and biological entities with specific and finely tuned functions for a broad range of applications in diagnosis and treatment.

Finally, concerning the architecture of FsNMs, it is necessary to explore the advantages provided by new techniques. For example, a procedure to obtain perforated nanosheets at the nanometric scale has been recently reported, as discussed above. However, the enormous potentiality of these FsNMs remains completely unknown from a technological point of view. Moreover, much effort needs to be devoted to integrating new techniques for modifying or patterning the surface of nanosheets not only in already developed biomedical applications, but also in the development of new ones. For example, surface modification to functionalize and/or re-orient polymer molecules in ECP-containing nanosheets is expected to offer numerous opportunities as active biomedical interfaces.

In summary, numerous scientific and technical challenges for the design of FsNM abound, and it can be foreseen that their development for biomedical applications will continue to be a research area of growing interest.

Acknowledgements

The authors are in debt to support from MINECO and FEDER (MAT2012-34498 and MAT2012-36205) and Generalitat de Catalunya (XRQTC). M.M.P.-M. thanks financial support through a FPI-UPC grant.

References

1 R. Langer, *J. Biomed. Mater. Res., Part A*, 2013, **101**, 2449.
2 S. Fleischer and T. Dvir, *Curr. Opin. Biotechnol.*, 2013, **24**, 664.
3 T. Cohen-Karni, R. Langer and D. S. Kohane, *ACS Nano*, 2012, **6**, 6541.
4 C. Jiang, S. Markutsya, Y. Pikus and V. V. Tsukruk, *Nat. Mater.*, 2004, **3**, 721.
5 J. D. Kittle, C. Wang, C. Qian, Y. Zhang, M. Zhang, M. Roman, J. R. Morris, R. B. Moore and A. R. Esker, *Biomacromolecules*, 2012, **13**, 714.
6 M. G. Bellino, I. Tropper, H. Duran, A. E. Regazzoni and G. J. A. A. Soler-Illia, *Small*, 2010, **6**, 1221.
7 J. A. Jaber, P. B. Chase and J. B. Schlenoff, *Nano Lett.*, 2003, **3**, 1505.
8 C. S. Hajicharalambous, J. Lichter, W. T. Hix, M. Swierczewska, M. F. Rubner and P. Rajagopalan, *Biomaterials*, 2009, **30**, 4029.
9 Z. Tai, H. Ma, B. Liu, X. Yan and Q. Xue, *Colloids Surf., B*, 2012, **89**, 147.
10 S. Y. Wong, Q. Li, J. Veselinovic, B.-S. Kim, A. M. Klibanov and P. T. Hammond, *Biomaterials*, 2010, **31**, 4079.
11 M. C. Berg, L. Zhai, R. E. Cohen and M. F. Rubner, *Biomacromolecules*, 2006, **7**, 357.
12 K. C. Wood, J. Q. Boedicker, D. M. Lynn and P. T. Hammond, *Langmuir*, 2005, **21**, 1603.
13 H. Watanabe, E. Muto, T. Ohzono, A. Nakao and T. Kunitake, *J. Mater. Chem.*, 2009, **19**, 2425.
14 Handbook of Nanophysics, *Functional Nanomaterials*, ed. K. D. Sattler, CRC Press, Taylor and Francis Group, Boca Raton, FL, 2011, vol. 5.
15 G. Decher, J. D. Hong and J. Schmitt, *Thin Solid Films*, 1992, **210–211**, 831.
16 G. Decher, *Science*, 1997, **277**, 1232.
17 G. Decher, Y. Lvov and J. Schmitt, *Thin Solid Films*, 1994, **244**, 772.
18 R. W. Corkery, *Langmuir*, 1997, **13**, 3591.
19 D. B. Hall, P. Underhill and J. M. Torkelson, *Polym. Eng. Sci.*, 1998, **38**, 2039.
20 I. Gurrappa and L. Binder, *Sci. Technol. Adv. Mater.*, 2008, **9**, 043001.

 This journal is © The Royal Society of Chemistry 2015

Open Access Article. Published on 28 May 2015. Downloaded on 4/2/2026 11:03:23 AM.
This article is licensed under a Creative Commons Attribution 3.0 Unported Licence.

21 A. D. Stroock, R. S. Kane, M. Weck, S. J. Metallo and G. M. Whitesides, *Langmuir*, 2002, **19**, 2466.
22 W. Cheng, M. J. Campolongo, S. J. Tan and D. Luo, *Nano Today*, 2009, **4**, 482.
23 C. Jiang and V. V. Tsukruk, *Adv. Mater.*, 2006, **18**, 829.
24 T. A. Skotheim, R. L. Elsenbaumer and J. R. Reynolds, *Handb. Conduct. Polym.*, Marcel Dekker, New York, 1998.
25 C. Li, C. Bai and G. Shi, *Chem. Soc. Rev.*, 2009, **38**, 2397.
26 D. W. Hatchett and M. Josowicz, *Chem. Rev.*, 2008, **108**, 746.
27 J. L. Bredas and G. B. Street, *Acc. Chem. Res.*, 1985, **18**, 309.
28 B. A. Bolto, R. McNeill and D. E. Weiss, *Aust. J. Chem.*, 1963, **16**, 1090.
29 H. Shirakawa, E. J. Louis, A. G. MacDiarmid, C. K. Chiang and A. J. Heeger, *J. Chem. Soc., Chem. Commun.*, 1977, 578.
30 Y. Xu, F. Zhang and X. Feng, *Small*, 2011, **7**, 1338.
31 B. Kippelen and J.-L. Brédas, *Energy Environ. Sci.*, 2009, **2**, 251.
32 Y. Xuan, M. Sandberg, M. Berggren and X. Crispin, *Org. Electron.*, 2012, **13**, 632.
33 D. Aradilla, F. Estrany, F. Casellas, J. I. Iribarren and C. Alemán, *Org. Electron.*, 2014, **15**, 40.
34 D. Aradilla, J. Casanovas, F. Estrany, J. I. Iribarren and C. Alemán, *Polym. Chem.*, 2012, **3**, 436.
35 H.-E. Yin, C.-H. Wu, K.-S. Kuo, W.-Y. Chiu, C.-F. Lee, N.-T. Li and P.-J. Chen, *Synth. Met.*, 2011, **161**, 1878.
36 N. K. Guimard, N. Gomez and C. E. Schmidt, *Prog. Polym. Sci.*, 2007, **32**, 876.
37 A.-D. Bendrea, L. Cianga and I. Cianga, *J. Biomater. Appl.*, 2011, **26**, 3.
38 R. Ravichandran, S. Sundarrajan, J. R. Venugopal, S. Mukherjee and S. Ramakrishna, *J. R. Soc., Interface*, 2010, **7**, S559.
39 J. Jaguar-Grodzinski, *e-Polym.*, 2012, **12**, 722.
40 C. Rincón and J. C. Meredith, *Macromol. Biosci.*, 2010, **10**, 258.
41 L. J. del Valle, F. Estrany, E. Armelin, R. Oliver and C. Alemán, *Macromol. Biosci.*, 2008, **8**, 1144.
42 L. J. del Valle, D. Aradilla, R. Oliver, F. Sepulcre, A. Gamez, E. Armelin, C. Alemán and F. Estrany, *Eur. Polym. J.*, 2007, **43**, 2342.
43 B. Guo, L. Glavas and A.-C. Albertsson, *Prog. Polym. Sci.*, 2013, **38**, 1263.
44 G. Shi, M. Rouabhia, Z. Wang, L. H. Dao and Z. Zhang, *Biomaterials*, 2004, **25**, 2477.
45 L. Huang, X. Zhuang, J. Hu, L. Lang, P. Zhang, Y. Wang, X. Chen, Y. Wei and X. Jing, *Biomacromolecules*, 2008, **9**, 850.
46 S. I. Jeong, I. D. Jun, M. J. Choi, Y. C. Nho, Y. M. Lee and H. Shin, *Macromol. Biosci.*, 2008, **8**, 627.
47 E. Llorens, M. M. Pérez-Madrigal, E. Armelin, L. J. del Valle, J. Puiggalí and C. Alemán, *RSC Adv.*, 2014, **4**, 15245.
48 M. Planellas, M. M. Pérez-Madrigal, L. J. del Valle, S. Kobauri, R. Katsarava, C. Alemán and J. Puiggalí, *Polym. Chem.*, 2015, **6**, 925.
49 J. H. Hardy, D. J. Mouser, N. Arroyo-Currás, S. Geissler, J. K. Chow, L. Nguy, J. M. Kim and C. E. Schmidt, *J. Mater. Chem. B*, 2014, **2**, 6809.
50 K. M. Nampoothiri, N. R. Nair and R. P. John, *Bioresour. Technol.*, 2010, **101**, 8493.
51 K. Odelius, P. Plikk and A.-C. Albertsson, *Biomacromolecules*, 2005, **6**, 2718.
52 F. Khan and S. R. Ahmad, *Macromol. Biosci.*, 2013, **13**, 395.
53 R. Parenteau-Bareil, R. Gauvin and F. Berthod, *Materials*, 2010, **3**, 1863.
54 S. Martino, F. D'Angelo, I. Armentano, J. M. Kenny and A. Orlacchio, *Biotechnol. Adv.*, 2012, **30**, 338.
55 C. Zhao, A. Tan, G. Pastorin and H. K. Ho, *Biotechnol. Adv.*, 2013, **31**, 654.
56 Y. Okamura, K. Kabata, M. Kinoshita, D. Saitoh and S. Takeoka, *Adv. Mater.*, 2009, **21**, 4388.
57 K. Fujino, M. Kinoshita, A. Saitoh, H. Yano, K. Nishikawa, T. Fujie, K. Iwaya, M. Kakihara, S. Takeoka, D. Saitoh and Y. Tanaka, *Surg. Endosc.*, 2011, **25**, 3428.
58 H. Miyazaki, M. Kinoshita, A. Saito, T. Fujie, K. Kabata, E. Hara, S. Ono, S. Takeoka and D. Saitoh, *Wound Repair Regen.*, 2012, **20**, 573.
59 Y. Okamura, K. Kabata, M. Kinoshita, H. Miyazaki, A. Saito, T. Fujie, S. Ohtsubo, D. Saitoh and S. Takeoka, *Adv. Mater.*, 2013, **25**, 545.
60 V. Pensabene, S. Taccola, L. Ricotti, G. Ciofani, A. Menciassi, F. Perut, M. Salerno, P. Dario and N. Baldini, *Acta Biomater.*, 2011, **7**, 2883.
61 L. Ricotti, S. Taccola, V. Pensabene, V. Mattoli, T. Fujie, S. Takeoka, A. Menciassi and P. Dario, *Biomed. Microdevices*, 2010, **12**, 809.
62 T. Fujie, L. Ricotti, A. Desii, A. Menciassi, P. Dario and V. Mattoli, *Langmuir*, 2011, **27**, 13173.
63 D. Niwa, T. Fujie, T. Lang, N. Goda and S. Takeoka, *J. Biomater. Appl.*, 2012, **27**, 131.
64 S. Taccola, A. Desii, V. Pensabene, T. Fujie, A. Saito, S. Takeoka, P. Dario, A. Menciassi and V. Mattoli, *Langmuir*, 2011, **27**, 5589.
65 D. Chen, J. Chen, M. Wu, H. Tian, X. Chen and J. Sun, *Langmuir*, 2013, **29**, 8328.
66 Y. Okamura, Y. Fukui, K. Kabata, H. Suzuki, M. Handa, Y. Ikeda and S. Takeoka, *Bioconjugate Chem.*, 2009, **20**, 1958.
67 S. Boddohi and M. J. Kipper, *Adv. Mater.*, 2010, **22**, 2998.
68 T. Fujie, Y. Okamura and S. Takeoka, *Adv. Mater.*, 2007, **19**, 3549.
69 S. Takeoka, Y. Okamura, T. Fujie and Y. Fukui, *Pure Appl. Chem.*, 2008, **80**, 2259.
70 T. Fujie, N. Matsutani, M. Kinoshita, Y. Okamura, A. Saito and S. Takeoka, *Adv. Funct. Mater.*, 2009, **19**, 2560.
71 T. Fujie, M. Kinoshita, S. Shono, A. Saito, Y. Okamura, D. Saitoh and S. Takeoka, *Surgery*, 2010, **148**, 48.
72 T. Fujie, A. Saito, M. Kinoshita, H. Miyazaki, S. Ohtsubo, D. Saitoh and S. Takeoka, *Biomaterials*, 2010, **31**, 6269.
73 A. Saito, H. Miyazaki, T. Fujie, S. Ohtsubo, M. Kinoshita, D. Saitoh and S. Takeoka, *Acta Biomater.*, 2012, **8**, 2932.
74 K. Hagisawa, A. Saito, M. Kinoshita, T. Fujie, N. Otani, S. Shono, Y.-K. Park and S. Takeoka, *J. Vasc. Surg. Venous Lymphat. Disord.*, 2013, **1**, 289.

Open Access Article. Published on 28 May 2015. Downloaded on 4/2/2026 11:03:23 AM.
This article is licensed under a Creative Commons Attribution 3.0 Unported Licence.

75 N. Otani, M. Kinoshita, T. Fujie, A. Saito, S. Takeoka, D. Saitoh, K. Hagisawa, H. Nawashiro and K. Shima, *J. Clin. Neurosci.*, 2013, **20**, 301.
76 T. Fujie, S. Furutate, D. Niwa and S. Takeoka, *Soft Matter*, 2010, **6**, 4672.
77 C. Picart, J. Mutterer, L. Richert, Y. Luo, G. D. Prestwich, P. Schaaf, J.-C. Voegel and P. Lavalle, *Proc. Natl. Acad. Sci. U. S. A.*, 2002, **99**, 12531.
78 J. Chen, X. Qiu, L. Wang, W. Zhong, J. Kong and M. M. Q. Xing, *Adv. Funct. Mater.*, 2014, **24**, 2216.
79 P. T. Hammond, *Adv. Mater.*, 2004, **16**, 1271.
80 F. Caruso, R. A. Caruso and H. Möhwald, *Science*, 1998, **282**, 1111.
81 M. Matsusaki, K. Kadowaki, T. Nakahara and M. Akashi, *Angew. Chem., Int. Ed.*, 2007, **46**, 4689.
82 L. Ma, D. Li and J. Chen, *Drug Dev. Ind. Pharm.*, 2014, **40**, 845.
83 B. L. Seal, T. C. Otero and A. Panitch, *Mater. Sci. Eng., R*, 2001, **34**, 147.
84 L. Moroni, J. R. de Wijn and C. A. van Blitterswijk, *J. Biomater. Sci., Polym. Ed.*, 2008, **19**, 543.
85 J. L. Lutkenhaus, K. D. Hrabak, K. McEnnis and P. T. Hammond, *J. Am. Chem. Soc.*, 2005, **127**, 17228.
86 S. S. Ono and G. Decher, *Nano Lett.*, 2006, **6**, 592.
87 N. Meyerbröker, Z.-A. Li, W. Eck and M. Zharnikov, *Chem. Mater.*, 2012, **24**, 2965.
88 N. Meyerbröker and M. Zharnikov, *Adv. Mater.*, 2014, **26**, 3328.
89 N. Meyerbröker, T. Kriesche and M. Zharnikov, *ACS Appl. Mater. Interfaces*, 2013, **5**, 2641.
90 F. Mallwitz and W. A. Goedel, *Angew. Chem., Int. Ed.*, 2001, **40**, 2645.
91 Y. Ma, J. Sun and J. Shen, *Chem. Mater.*, 2007, **19**, 5058.
92 Z. Gui, J. Qian, B. Du, M. Yin and Q. An, *J. Colloid Interface Sci.*, 2009, **340**, 35.
93 S. T. Dubas, T. R. Farhat and J. B. Schlenoff, *J. Am. Chem. Soc.*, 2001, **123**, 5368.
94 M. Kohri, Y. Shinoda, H. Kohma, Y. Nannichi, M. Yamauchi, S. Yagai, T. Kojima, T. Taniguchi and K. Kishikawa, *Macromol. Rapid Commun.*, 2013, **34**, 1220.
95 T. Fujie, H. Haniuda and S. Takeoka, *J. Mater. Chem.*, 2011, **21**, 9112.
96 T. Fujie, A. Desii, L. Ventrelli, B. Mazzolai and V. Mattoli, *Biomed. Microdevices*, 2012, **14**, 1069.
97 H. Zhang and S. Takeoka, *Macromolecules*, 2012, **45**, 4315.
98 T. Fujie, S. Ahadian, H. Liu, H. Chang, S. Ostrovidov, H. Wu, H. Bae, K. Nakajima, H. Kaji and A. Khademhosseini, *Nano Lett.*, 2013, **13**, 3185.
99 C. Jiang, S. Markutsya and V. V. Tsukruk, *Adv. Mater.*, 2004, **16**, 157.
100 L. Shen, B. Wang, J. Wang, J. Fu, C. Picart and J. Ji, *ACS Appl. Mater. Interfaces*, 2012, **4**, 4476.
101 S. Y. Wong, Q. Li, J. Veselinovic, B.-S. Kim, A. M. Klibanov and P. T. Hammond, *Biomaterials*, 2010, **31**, 4079.
102 S. H. Baxamusa, M. Stadermann, C. Aracne-Ruddle, A. J. Nelson, M. Chea, S. Li, K. Youngblood and T. I. Suratwala, *Langmuir*, 2014, **30**, 5126.
103 L. B. Freund and S. Suresh, *Thin Film Materials: Stress, Defect Formation and Surface Evolution*, Cambridge University Press, Cambridge, UK, 2003.
104 H. Qin, D. Wang, X. Xiong and J. Jin, *Macromol. Rapid Commun.*, 2014, **35**, 1055.
105 P. R. Bidez, S. Li, A. G. MacDiarmid, E. C. Venancio, Y. Wei and P. I. Lelkes, *J. Biomater. Sci., Polym. Ed.*, 2006, **17**, 199.
106 I. Jun, S. Jeong and H. Shin, *Biomaterials*, 2009, **30**, 2038.
107 J. Huang, X. Hu, L. Lu, Z. Ye, Q. Zhang and Z. Luo, *J. Biomed. Mater. Res., Part A*, 2010, **93**, 164.
108 J. Y. Lee, C. A. Bashur, C. A. Milroy, L. Forciniti, A. S. Goldstein and C. E. Schmidt, *IEEE Trans. Nanobiosci.*, 2012, **11**, 15.
109 C. R. Broda, J. Y. Lee, S. Sirivisoot, C. E. Schmidt and B. S. Harrison, *J. Biomed. Mater. Res., Part A*, 2011, **98**, 509.
110 A.-D. Bendrea, G. Fabregat, J. Torras, S. Maione, L. Cianga, L. J. del Valle, I. Cianga and C. Alemán, *J. Mater. Chem. B*, 2013, **1**, 4135.
111 E. Llorens, M. M. Pérez-Madrigal, E. Armelin, L. J. del Valle, J. Puiggalí and C. Alemán, *RSC Adv.*, 2014, **4**, 15245.
112 D. E. López-Pérez, D. Aradilla, L. J. del Valle and C. Alemán, *J. Phys. Chem. C*, 2013, **117**, 6607.
113 B. Teixeira-Dias, L. J. del Valle, D. Aradilla, F. Estrany and C. Alemán, *Macromol. Mater. Eng.*, 2012, **297**, 427.
114 G. Fabregat, B. Teixeira-Dias, L. J. del Valle, E. Armelin, F. Estrany and C. Alemán, *ACS Appl. Mater. Interfaces*, 2014, **6**, 11940.
115 G. Fabregat, E. Armelin and C. Alemán, *J. Phys. Chem. B*, 2014, **118**, 4669.
116 M. Martí, G. Fabregat, F. Estrany, E. Armelin and C. Alemán, *J. Mater. Chem.*, 2010, **20**, 10652.
117 G. Fabregat, E. Córdova-Mateo, E. Armelin, O. Bertran and C. Alemán, *J. Phys. Chem. C*, 2011, **115**, 14933.
118 S. Radhakrishnan, C. Sumathi, A. Umar, S. J. Kim, J. Wilson and V. Dharuman, *Biosens. Bioelectron.*, 2013, **47**, 133.
119 B. Teixeiras-Dias, D. Zanuy, J. Poater, M. Solà, F. Estrany, L. J. del Valle and C. Alemán, *Soft Matter*, 2011, **7**, 9922.
120 E. Llorens, E. Armelin, M. M. Pérez-Madrigal, L. J. del Valle and C. Alemán, *Polymers*, 2013, **5**, 1115.
121 X. F. Lu, W. J. Zhang, C. Wang, T.-C. Wen and Y. Wei, *Prog. Polym. Sci.*, 2011, **36**, 671.
122 G. Fabregat, E. Córdova-Mateo, E. Armelin, O. Bertran and C. Alemán, *J. Phys. Chem. C*, 2011, **115**, 14933.
123 C. Z. Liao and F. Yan, *Polym. Rev.*, 2013, **3**, 352–406.
124 M. Marti, G. Fabregat, F. Estrany, C. Alemán and E. Armelin, *J. Mater. Chem.*, 2010, **20**, 10652.
125 L. Li, Y. Shi, L. J. Pan, Y. Shi and G. H. Yu, *J. Mater. Chem. B*, 2015, **3**, 2920.
126 L. Kergoat, B. Piro, D. T. Simon, M. C. Pham, V. Noel and M. Berggren, *Adv. Mater.*, 2014, **26**, 5658.
127 P. Humpolicek, V. Kasparkova, P. Saha and J. Stejskal, *Synth. Met.*, 2012, **162**, 722.
128 C. H. Wang, Y. Q. Dong, K. Sengothi, K. L. Tan and E. T. Kang, *Synth. Met.*, 1999, **102**, 1313.
129 M. Mattioli-Belmonte, G. Giavaresi, G. Biagini, L. Virgili, M. Giacomini, M. Fini, F. Giantomassi, D. Natali,

 This journal is © The Royal Society of Chemistry 2015

Open Access Article. Published on 28 May 2015. Downloaded on 4/2/2026 11:03:23 AM.
This article is licensed under a Creative Commons Attribution 3.0 Unported Licence.

P. Torricelli and R. Giardino, *Int. J. Artif. Organs*, 2003, **23**, 1077.
130 X. Wang, X. Gu, C. Yuan, S. Chen, P. Zhang, T. zhang, J. Yao, F. Chen and G. Chen, *J. Biomed. Mater. Res., Part A*, 2004, **68**, 411.
131 P. M. George, A. w. Lyckman, D. A. LaVan, A. Hedge, Y. Leung, R. Avasare, C. Testa, P. M. Alexander, R. Langer and M. Sur, *Biomaterials*, 2005, **26**, 3511.
132 S. Maione, G. Fabregat, L. J. del Valle, A.-D. Bendrea, L. Cianga, I. Cianga, I. F. Estrany and C. Alemán, *J. Polym. Sci., Part B: Polym. Phys.*, 2015, **53**, 239.
133 F. Wang, M. Li, B. Wang, J. Zhang, Y. Cheng, L. Liu, F. Lv and S. Wang, *Sci. Rep.*, 2015, **5**, 7617.
134 S. Yin, Y. Goldovsky, M. Herzberg, L. Liu, H. Sun, Y. Zhang, F. Meng, X. Cao, D. D. Sun, H. Chen, A. Kushmaro and X. Chen, *Adv. Funct. Mater.*, 2013, **23**, 2971.
135 T. Nishikawa, R. Ookura, J. Nishida, K. Arai, J. Hayashi, N. Kurono, T. Sawadaishi, M. Hara and M. Shimomura, *Langmuir*, 2002, **18**, 5734.
136 Y. Zhang, T. R. Nayak, H. Hong and W. Cai, *Nanoscale*, 2012, **4**, 3833.
137 Y. Yang, A. M. Asiri, Z. Tang, D. Du and Y. Lin, *Mater. Today*, 2013, **16**, 365.
138 J. Lei, Z. Li, X. Lu, W. Wang, X. Bian, T. Zheng, Y. Xue and C. Wang, *J. Colloid Interface Sci.*, 2011, **364**, 555.
139 T. F. Otero and M. J. Ariza, *J. Phys. Chem. B*, 2003, **107**, 13954.
140 D. Chowdhury, A. Paul and A. Chattopadhyay, *Langmuir*, 2005, **21**, 4123.
141 Y. Lu, G. Shi, C. Li and Y. Liang, *J. Appl. Polym. Sci.*, 1998, **70**, 2169.
142 J. Song, H. Liu, M. Wan, Y. Zhu and L. Jiang, *J. Mater. Chem. A*, 2013, **1**, 1740.
143 B. Zhao, K. G. Neoh, F. T. Liu and E. T. Kang, *Langmuir*, 1999, **15**, 8259.
144 I. Mihai, F. Addiego, D. Ruch and V. Ball, *Sens. Actuators, B*, 2014, **192**, 769.
145 G.-W. Huang, H.-M. Xiao, H.-Q. Shi and S.-Y. Fu, *J. Polym. Sci., Part A: Polym. Chem.*, 2012, **50**, 2794.
146 R. Yue, S. Chen, B. Lu, C. Liu and J. Xu, *J. Solid State Electrochem.*, 2011, **15**, 539.
147 H. Zhu, L. Gao, M. Li, H. Yin and D. Wang, *Electrochem. Commun.*, 2011, **13**, 1479.
148 G. Shi, S. Jin, G. Xue and C. Li, *Science*, 1995, **267**, 994.
149 D. Wang, Y.-X. Li, Z. Shi, H.-L. Qin, L. Wang, X.-F. Pei and J. Jin, *Langmuir*, 2010, **26**, 14405.
150 S. S. Jeon, H. H. An, C. S. Yoon and S. S. Im, *Polymer*, 2011, **52**, 652.
151 G. Qi, L. Huang and H. Wang, *Chem. Commun.*, 2012, **48**, 8246.
152 P. Jha, S. P. Koiry, V. Saxena, P. Veerender, A. K. Chauhan, D. K. Aswal and S. K. Gupta, *Macromolecules*, 2011, **44**, 4583.
153 Z. Tong, Y. Yang, J. Wang, J. Zhao, B.-L. Su and Y. Li, *J. Mater. Chem. A*, 2014, **2**, 4642.
154 Z. Niu, P. Luan, Q. Shao, H. Dong, J. Li, J. Chen, D. Zhao, L. Cai, W. Zhou, X. Chen and S. Xie, *Energy Environ. Sci.*, 2012, **5**, 8726.
155 F. Greco, A. Zucca, S. Taccola, A. Menciassi, T. Fujie, H. Haniuda, S. Takeoka, P. Dario and V. Mattoli, *Soft Matter*, 2011, **7**, 10642.
156 M. H. Bolin, K. Svennersten, X. Wang, I. S. Chronakis, A. Richter-Dahlfors, E. W. H. Jager and M. Berggren, *Sens. Actuators, B*, 2009, **142**, 451.
157 K. Svennersten, M. H. Bolin, E. W. H. Jager, M. Berggren and A. Richter-Dahlfors, *Biomaterials*, 2009, **30**, 6257.
158 S. Taccola, F. Greco, B. Mazzolai, V. Mattoli and E. W. H. Jager, *J. Micromech. Microeng.*, 2013, **23**, 117004.
159 S. Taccola, F. Greco, A. Zucca, C. Innocenti, C. de Julián Fernández, G. Campo, C. Sangregorio, B. Mazzolai and V. Mattoli, *ACS Appl. Mater. Interfaces*, 2013, **5**, 6324.
160 F. Greco, T. Fujie, L. Ricotti, S. Taccola, B. Mazzolai and V. Mattoli, *ACS Appl. Mater. Interfaces*, 2013, **5**, 573.
161 C.-C. Fu, A. Grimes, M. Long, C. G. L. Ferri, B. D. Rich, S. Ghosh, S. Ghosh, L. P. Lee, A. Gopinathan and M. Khine, *Adv. Mater.*, 2009, **21**, 4472.
162 J. A. Lee, M. K. Shin, S. H. Kim, S. J. Kim, G. M. Spinks, G. G. Wallace, R. Ovalle-Robles, M. D. Lima, M. E. Kozlov and R. H. Baughman, *ACS Nano*, 2012, **6**, 327.
163 O. Ahumada, M. M. Pérez-Madrigal, J. Ramirez, D. Curcó, C. Esteves, A. Salvador-Matar, G. Luongo, E. Armelin, J. Puiggalí and C. Alemán, *Rev. Sci. Instrum.*, 2013, **84**, 053904.
164 A. L. Gomes, J. Casanovas, O. Bertran, J. S. de C. Campos, E. Armelin and C. Alemán, *J. Polym. Res.*, 2011, **18**, 1509.
165 R. A. Khalkhali and M. B. Keivani, *Asian J. Chem.*, 2005, **17**, 835.
166 J. A. Marins, B. G. Soares, M. Fraga, D. Müller and G. M. O. Barra, *Cellulose*, 2014, **21**, 1409.
167 E. Armelin, A. L. Gomes, M. M. Pérez-Madrigal, J. Puiggalí, L. Franco, L. J. del Valle, A. Rodríguez-Galán, J. S. d. C. Campos, N. Ferrer-Anglada and C. Alemán, *J. Mater. Chem.*, 2012, **22**, 585.
168 M. M. Pérez-Madrigal, E. Armelin, L. J. del Valle, F. Estrany and C. Alemán, *Polym. Chem.*, 2012, **3**, 979.
169 M. M. Pérez-Madrigal, M. I. Giannotti, G. Oncins, L. Franco, E. Armelin, J. Puiggalí, F. Sanz, L. J. del Valle and C. Alemán, *Polym. Chem.*, 2013, **4**, 568.
170 M. M. Pérez-Madrigal, M. I. Giannotti, E. Armelin, F. Sanz and C. Alemán, *Polym. Chem.*, 2014, **5**, 1248.
171 M. M. Pérez-Madrigal, M. I. Giannotti, L. J. del Valle, L. Franco, E. Armelin, J. Puiggalí, F. Sanz and C. Alemán, *ACS Appl. Mater. Interfaces*, 2014, **6**, 9719.
172 F. Greco, A. Zucca, S. Taccola, B. Mazzolai and V. Mattoli, *ACS Appl. Mater. Interfaces*, 2013, **5**, 9461.
173 J. George, J. Onodera and T. Miyata, *J. Biomed. Mater. Res., Part A*, 2008, **87**, 1103.
174 J. George, Y. Kuboki and T. Miyata, *Biotechnol. Bioeng.*, 2006, **95**, 404.
175 D. J. Kim, M. J. Jo and S. Y. Nam, *J. Ind. Eng. Chem.*, 2015, **21**, 36.
176 R. Holze and Y. P. Wu, *Electrochim. Acta*, 2014, **122**, 93.
177 R. K. Pandey and V. Lakshminarayanan, *J. Phys. Chem. C*, 2009, **113**, 21596.

Open Access Article. Published on 28 May 2015. Downloaded on 4/2/2026 11:03:23 AM.
This article is licensed under a Creative Commons Attribution 3.0 Unported Licence.

178 B. Rajesh, K. R. Thampi, J. M. Bonard, A. J. McEvoy, N. Xanthopoulus, H. J. Mathieu and B. Viswanathan, *J. Power Sources*, 2004, **133**, 155.
179 J.-D. Qiu, L. Shi, R. P. Liang, G.-C. Wang and X. H. Xia, *Chem. – Eur. J.*, 2012, **18**, 7950.
180 C. Arbizzani, M. Biso, E. Manferrari and M. Mastragostino, *J. Power Sources*, 2008, **180**, 41.
181 C. Arbizzani, M. Biso, E. Manferrari and M. Mastragostino, *J. Power Sources*, 2008, **178**, 584.
182 A. Kraytsbergs and Y. Ein-Eli, *Energy Fuels*, 2014, **28**, 7303.
183 T. F. Otero, E. Angulo, J. Rodriguez and C. Santamaria, *J. Electroanal. Chem.*, 1992, **341**, 369.
184 Q. B. Pei and O. Inganäs, *Adv. Mater.*, 1992, **4**, 277.
185 E. W. H. Jager, E. Smela and O. Inganäs, *Science*, 2000, **290**, 1540.
186 E. W. H. Jager, O. Inganäs and I. Lundstrom, *Science*, 2000, **288**, 2335.
187 S. D. Deshpande, J. Kim and S. R. Yun, *Smart Mater. Struct.*, 2005, **14**, 876.
188 S. J. Higgins, K. V. Lovell, R. M. G. Rajapakse and N. M. Walsby, *J. Mater. Chem.*, 2003, **13**, 2485.
189 G. Alici, A. Punning and H. R. Shea, *Sens. Actuators, B*, 2011, **157**, 72.
190 L. Valero Conzuelo, J. Arias-Pardilla, J. V. Cauigh-Rodríguez, M. A. Smit and T. F. Otero, *Sensors*, 2010, **10**, 2638.
191 T. F. Otero, J. G. Martínez and J. Arias-Pardilla, *Electrochim. Acta*, 2012, **84**, 112–128.

 This journal is © The Royal Society of Chemistry 2015